Available online at www.sciencedirect.com
ScienceDirect
Journal of Sound and Vibration 325 (2009) 186–205
JOURNAL OF SOUND AND VIBRATION
www.elsevier.com/locate/jsvi

Active control of geometrically nonlinear vibrations of functionally graded laminated composite plates using piezoelectric fiber reinforced composites

Satyajit Panda, M.C. Ray*

Department of Mechanical Engineering, Indian Institute of Technology, Kharagpur 721302, India

Received 28 July 2008; received in revised form 26 February 2009; accepted 7 March 2009
Handling Editor: J. Lam
Available online 8 May 2009

Abstract

This paper deals with the geometrically nonlinear dynamic analysis of functionally graded (FG) laminated composite plates integrated with a patch of active constrained layer damping (ACLD) treatment. The constraining layer of the ACLD treatment is considered to be made of the piezoelectric fiber reinforced composite (PFRC) material. Each layer of the substrate FG laminated composite plate is made of fiber-reinforced composite material in which the fibers are longitudinally aligned in the plane parallel to the top or bottom surface of the layer and the layer is assumed to be graded in the thickness direction by way of varying the fiber orientation angle across its thickness according to a power-law. The novelty of the present work is that, unlike the traditional laminated composite plates, the FG laminated composite plates are constructed in such a way that the continuous variation of material properties and stresses across the thickness of the plates is achieved. The constrained viscoelastic layer of the ACLD treatment is modeled using the Golla–Hughes–McTavish (GHM) method. Based on the first-order shear deformation (FSDT) theory, a finite element model has been developed to model the open-loop and closed-loop nonlinear dynamics of the overall FG laminated composite plates. Both symmetric and asymmetric FG laminated composite plates are considered as the substrate plates for presenting the numerical results. The analysis suggests the potential use of the ACLD treatment with its constraining layer made of the PFRC material for active control of geometrically nonlinear forced vibrations of FG laminated composite plates. The effect of piezoelectric fiber orientation in the active constraining PFRC layer on the damping characteristics of the overall FG plates is also investigated.

1. Introduction

In recent years, a new class of non-homogeneous composite materials known as ''functionally graded materials'' (FGMs) has earned a considerable attention in structural applications. These materials are characterized by a smooth and continuous variation of material properties particularly along the thickness direction. In an endeavor to develop the super heat resistant materials, Koizumi [1] first proposed the concept

*Corresponding author. Tel.: +91 3222 55221.
E-mail address: mcray@mech.iitkgp.ernet.in (M.C. Ray).

0022-460X/$ - see front matter © 2009 Elsevier Ltd. All rights reserved.
doi:10.1016/j.jsv.2009.03.016

of this FGM. These materials are typically made from isotropic components, such as metals and ceramics and as a whole considered as isotropic functionally graded (FG) material. A great deal of research has already been reported on the buckling analysis [2], exact solutions [3–6], dynamic analysis [7–12] and nonlinear thermo-elastic analysis [13–15] of structures made of isotropic FG materials during the past few years.

The laminated composite structures can be tailored to design advanced structures but the sharp change in properties of each layer at the interface between the two adjacent layers causes large interlaminar shear stresses that eventually may give rise to the initiation of imperfection like delamination. Such detrimental effect can be mitigated using the FG lamina such that the properties of the laminated structure vary in a continuous manner along its thickness direction. The lamina of conventional unidirectional fiber-reinforced composite material may be tailored in such a way that the fibers are longitudinally aligned in the plane parallel to its top or bottom surface but the fiber orientation is assumed to vary in between its top and bottom surfaces according to a power-law [13,14] in order to attain the graded material properties along the thickness direction. The resulting lamina becomes an anisotropic lamina from analysis point of view and its properties at any point can be determined from nine independent material properties of the orthotropic lamina made of unidirectional fiber-reinforced composite material. Thus, this lamina may be called as a generally orthotropic FG lamina having the graded properties along its thickness direction. If this lamina is utilized to build a laminated composite structure such that the fiber orientation angles at the interface between two adjacent layers are identical then the material properties of the resulting laminated composite structure vary along the thickness direction in a continuous manner. Such a laminated composite structure may be called as a FG laminated composite structure.

In the quest for developing lightweight high performing flexible structures with self-controlling and/or self-monitoring capabilities, the piezoelectric materials are extensively used by exploiting its converse and direct piezoelectric effects as distributed actuators or sensors which are mounted on or embedded in the host structure [16,17]. Considerable interest has also been focused on investigating the performance of the functionally graded plates integrated with the piezoelectric actuators [18–20]. Further investigation on the efficient active control of the flexible structures using piezoelectric materials led to the development of active constrained layer damping (ACLD) treatment [21]. The ACLD treatment consists of a layer of viscoelastic material constrained between a host structure and an active constraining layer made of piezoelectric material. During the flexural vibration of the host structures, the active constraining layer not only restrains the constrained viscoelastic layer to undergo transverse shear deformations but also enhances the transverse shear deformations to cause improved damping characteristics of the overall structure over the conventional passive constrained layer damping (PCLD) treatment. Hence, the ACLD treatment has earned wide acceptability for efficient and reliable control of flexible structures [22–27].

Piezoelectric composite materials have emerged as the new class of smart materials and find wide applications as distributed actuators and sensors. Recently, Ray et al. [28,29] developed a new piezoelectric fiber reinforced composite (PFRC). The constructional feature of this PFRC material is that the monolithic piezoelectric fibers are longitudinally reinforced in the conventional epoxy matrix material. The effective piezoelectric coefficient e_{31} of this PFRC material, which quantifies the induced normal stress in the fiber direction due to the applied electric field in the direction transverse to the fiber direction is significantly larger than the corresponding coefficient of the piezoelectric material of the fibers. Note that if the in-plane actuation of the active piezoelectric constraining layer is utilized for active damping of smart structures then the performance of the ACLD treatment mainly depends on this piezoelectric coefficient (e_{31}).

In an attempt towards the development of new functionally graded smart structures using the isotropic FG materials, Ray and Sachade [30] first carried out the static analysis of simply supported isotropic FG plates integrated with a layer of this PFRC material. Panda and Ray [31] recently presented the analytical solutions for the geometrically nonlinear deformations of simply supported smart FG plates integrated with a distributed actuator made of PFRC material. Ray [32] carried out a linear frequency response analysis for active constrained layer damping of smart functionally graded plates using this PFRC material as the constraining layer of the ACLD treatment. Recently, Panda and Ray [33] investigated the ACLD of geometrically nonlinear vibrations of smart isotropic FG plates using PFRC material. In this paper, we consider FG laminated composite plates composed of generally orthotropic FG laminae as described earlier. ACLD of geometrically nonlinear forced vibrations of such FG laminated composite plates is investigated

using this PFRC material. A finite element model is developed to model the open-loop and closed-loop nonlinear dynamics of the FG laminated composite plates integrated with a patch of ACLD treatment. The constraining layer of the ACLD patch is made of the PFRC material as mentioned above. For the time domain analysis, the constrained viscoelastic layer of the ACLD treatment is modeled by the Golla–Hughes–McTavish (GHM) method [34,35]. The effect of piezoelectric fiber orientation angle in the PFRC constraining layer on the performance of the ACLD patch for controlling the nonlinear transient forced vibrations of the FG laminated composite plates has also been investigated. Both symmetric and asymmetric substrate FG laminated plates are considered as the numerical examples.

2. Finite element modeling

Fig. 1 illustrates a simply supported FG laminated composite plate integrated with a patch of ACLD treatment at the top surface of the substrate plate. The constraining layer of the ACLD treatment is made of the PFRC material. The substrate FG laminated composite plate is composed of N number of generally orthotropic FG lamina. The middle plane of the substrate plate is considered as the reference plane and the origin of the reference coordinate system is located at one corner of the reference plane such that the lines $x = 0,a$ and $y = 0,b$ represent the boundaries of the substrate FG laminated composite plate. The thickness of the host FG laminated composite plate, the viscoelastic constrained layer (($N+1$)-th layer) and the PFRC constraining layer (($N+2$)-th layer) are denoted by h, h_v and h_p, respectively. The piezoelectric fiber orientation in the active constraining layer of the PFRC material with respect to the reference coordinate system is denoted by ψ and the fibers are longitudinally aligned in the plane parallel to the xy-plane such that the in-plane actuation of the constraining layer causes transverse shear deformations of the constrained viscoelastic layer. Since the thickness of the overall plate is very thin, the first-order shear deformation (FSDT) theory is used to describe the kinematics of axial deformations as illustrated in Fig. 2. According to this kinematics of deformations, the axial displacements u and v at any point in the domain of the overall plate along x- and y-directions, respectively, can be expressed as

$$\begin{aligned} u(x,y,z,t) &= u_0(x,y,t) + (z - \langle z-h/2\rangle)\theta_x(x,y,t) + (\langle z-h/2\rangle - \langle z-h/2-h_v\rangle)\phi_x(x,y,t) \\ &\quad + \langle z-h/2-h_v\rangle\gamma_x(x,y,t) \\ v(x,y,z,t) &= v_0(x,y,t) + (z - \langle z-h/2\rangle)\theta_y(x,y,t) + (\langle z-h/2\rangle - \langle z-h/2-h_v\rangle)\phi_y(x,y,t) \\ &\quad + \langle z-h/2-h_v\rangle\gamma_y(x,y,t) \end{aligned} \tag{1}$$

where the brackets $\langle\ \rangle$ are used to define the appropriate singularity functions for satisfying the continuity condition between any two continua; u_0, v_0 are the generalized translational displacements of a point on the middle plane of the host FG laminated composite plate along x- and y-directions, respectively; θ_x, ϕ_x and γ_x are the generalized rotations of the normals to the mid-planes of the substrate FG laminated composite plate,

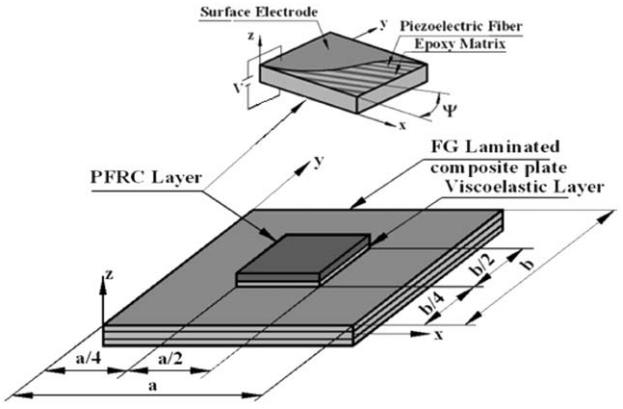

Fig. 1. Schematic diagram of a functionally graded laminated composite plate integrated with a patch of ACLD treatment.

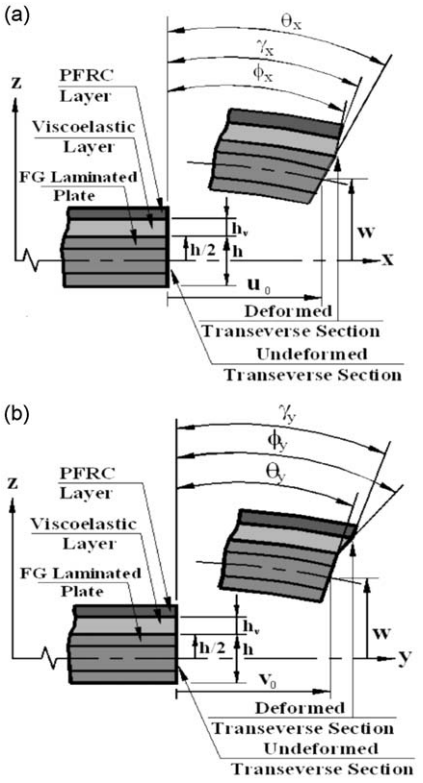

Fig. 2. Deformations of transverse cross-sections of the FG laminated composite plate integrated with the ACLD treatment which are parallel to: (a) *xz*- and (b) *yz*-planes.

the viscoelastic layer and the PFRC layer, respectively, about the *y*-axis; θ_y, ϕ_y and γ_y are the generalized rotations of these normals about the *x*-axis; The transverse displacement $w(x, y, t)$ at any point in the overall plate is assumed to be constant throughout the thickness of the overall FG laminated composite plate. For the ease of analysis, the generalized displacement variables are seperated into translational $\{\mathbf{d}_t\}$ and rotational $\{\mathbf{d}_r\}$ variables as follows:

$$\{\mathbf{d}_t\} = [u_0 \;\; v_0 \;\; w]^{\mathrm{T}} \quad \text{and} \quad \{\mathbf{d}_r\} = [\theta_x \;\; \theta_y \;\; \phi_x \;\; \phi_y \;\; \gamma_x \;\; \gamma_y]^{\mathrm{T}} \tag{2}$$

The state of strain at a point of the overall FG plate is defined by the following two strain vectors:

$$\{\boldsymbol{\varepsilon}_b\} = \{\varepsilon_x \;\; \varepsilon_y \;\; \varepsilon_{xy}\}^{\mathrm{T}} \quad \text{and} \quad \{\boldsymbol{\varepsilon}_s\} = \{\varepsilon_{xz} \;\; \varepsilon_{yz}\}^{\mathrm{T}} \tag{3}$$

where ε_x and ε_y are the normal strains along *x*- and *y*-directions, respectively; ε_{xy} is the in-plane shear strain; ε_{xz} and ε_{yz} are transverse shear strains. Similarly, the state of stress at any point of the overall plate is described by the following two stress vectors:

$$\{\boldsymbol{\sigma}_b\} = \{\sigma_x \;\; \sigma_y \;\; \sigma_{xy}\}^{\mathrm{T}} \quad \text{and} \quad \{\boldsymbol{\sigma}_s\} = \{\sigma_{xz} \;\; \sigma_{yz}\}^{\mathrm{T}} \tag{4}$$

in which σ_x and σ_y are the normal stresses along *x*- and *y*-directions, respectively, σ_{xy} is the in-plane shear stress, σ_{xz} and σ_{yz} are the transverse shear stresses. Considering the Green–Lagrange nonlinear strain–displacement relations for small strains and moderate rotations [36] and the displacement field given by Eq. (1), the strain vectors ($\{\boldsymbol{\varepsilon}_b\}, \{\boldsymbol{\varepsilon}_s\}$) and their first variations for the *k*-th layer of the overall laminated plate can be expressed as

$$\begin{Bmatrix} \{\boldsymbol{\varepsilon}_b^k\} \\ \{\boldsymbol{\varepsilon}_s^k\} \end{Bmatrix} = \begin{bmatrix} [\mathbf{L}_{bt}] & [\mathbf{Z}_b^k][\mathbf{L}_{br}] \\ [\mathbf{L}_{st}] & [\mathbf{Z}_s^k][\mathbf{L}_{sr}] \end{bmatrix} \begin{Bmatrix} \{\mathbf{d}_t\} \\ \{\mathbf{d}_r\} \end{Bmatrix} \quad \text{and} \quad \begin{Bmatrix} \{\boldsymbol{\delta\varepsilon}_b^k\} \\ \{\boldsymbol{\delta\varepsilon}_s^k\} \end{Bmatrix} = \begin{bmatrix} [\mathbf{L}_{bzt}] & [\mathbf{Z}_b^k][\mathbf{L}_{br}] \\ [\mathbf{L}_{st}] & [\mathbf{Z}_s^k][\mathbf{L}_{sr}] \end{bmatrix} \begin{Bmatrix} \{\boldsymbol{\delta}\mathbf{d}_t\} \\ \{\boldsymbol{\delta}\mathbf{d}_r\} \end{Bmatrix} \tag{5}$$

whereδ is an operator for first variation. Also, the operator matrices ($[\mathbf{L}_{bt}], [\mathbf{L}_{st}], [\mathbf{L}_{br}], [\mathbf{L}_{sr}], [\mathbf{L}_{b\alpha t}]$) and the transformation matrices ($[\mathbf{Z}_b^k], [\mathbf{Z}_s^k]$) appearing in Eq. (5) are given by

$$[\mathbf{L}_{bt}] = \begin{bmatrix} \partial/\partial x & 0 & 0 \\ 0 & \partial/\partial y & 0 \\ \partial/\partial y & \partial/\partial x & 0 \end{bmatrix} + \frac{1}{2}[\boldsymbol{\theta}] \begin{bmatrix} 0 & 0 & \partial/\partial x \\ 0 & 0 & \partial/\partial y \end{bmatrix}, \quad [\mathbf{L}_{st}] = \begin{bmatrix} 0 & 0 & \partial/\partial x \\ 0 & 0 & \partial/\partial y \end{bmatrix}$$

$$[\mathbf{L}_{br}] = \begin{bmatrix} \partial/\partial x & 0 & 0 & 0 & 0 & 0 & \partial/\partial y & 0 & 0 \\ 0 & 0 & 0 & \partial/\partial y & 0 & 0 & \partial/\partial x & 0 & 0 \\ 0 & \partial/\partial x & 0 & 0 & 0 & 0 & 0 & \partial/\partial y & 0 \\ 0 & 0 & 0 & 0 & \partial/\partial y & 0 & 0 & \partial/\partial x & 0 \\ 0 & 0 & \partial/\partial x & 0 & 0 & 0 & 0 & 0 & \partial/\partial y \\ 0 & 0 & 0 & 0 & 0 & \partial/\partial y & 0 & 0 & \partial/\partial x \end{bmatrix}^{\mathrm{T}},$$

$$[\mathbf{L}_{sr}] = \begin{bmatrix} 1 & 0 & 0 & 0 & 0 & 0 \\ 0 & 0 & 1 & 0 & 0 & 0 \\ 0 & 0 & 0 & 0 & 1 & 0 \\ 0 & 1 & 0 & 0 & 0 & 0 \\ 0 & 0 & 0 & 1 & 0 & 0 \\ 0 & 0 & 0 & 0 & 0 & 1 \end{bmatrix},$$

$$[\mathbf{L}_{b\alpha t}] = \begin{bmatrix} \partial/\partial x & 0 & 0 \\ 0 & \partial/\partial y & 0 \\ \partial/\partial y & \partial/\partial x & 0 \end{bmatrix} + [\boldsymbol{\theta}] \begin{bmatrix} 0 & 0 & \partial/\partial x \\ 0 & 0 & \partial/\partial y \end{bmatrix}, \quad [\boldsymbol{\theta}] = \begin{bmatrix} \partial w/\partial x & 0 \\ 0 & \partial w/\partial y \\ \partial w/\partial y & \partial w/\partial x \end{bmatrix},$$

$$[\mathbf{Z}_b^k] = [\mathbf{I}_b] \otimes \{\mathbf{z}_b^k\}, \quad [\mathbf{Z}_s^k] = [\mathbf{I}_s] \otimes \{\mathbf{z}_s^k\}, \quad k = 1, 2, \ldots, (N+2)$$

$$\{\mathbf{z}_b^k\} = [z \;\; 0 \;\; 0] \quad \text{and} \quad \{\mathbf{z}_s^k\} = [1 \;\; 0 \;\; 0] \quad \text{for} \quad k = 1, 2, \ldots, N$$

$$\{\mathbf{z}_b^k\} = [h/2 \;\; (z - h/2) \;\; 0] \quad \text{and} \quad \{\mathbf{z}_s^k\} = [0 \;\; 1 \;\; 0] \quad \text{for } k = (N+1),$$

$$\{\mathbf{z}_b^k\} = [h/2 \;\; h_v \;\; (z - h/2 - h_v)] \quad \text{and} \quad \{\mathbf{z}_s^k\} = [0 \;\; 0 \;\; 1] \quad \text{for } k = (N+2) \tag{6}$$

in which $[\mathbf{I}_b]$ and $[\mathbf{I}_s]$ are a 3×3 and a 2×2 identity matrices, respectively, and $\otimes$ denotes the Kronecker product. In the k-th layer of the host FG laminated composite plate, the fibers are longitudinally aligned in the plane parallel to the xy-plane but the fiber orientation angle with respect to the x-axis is assumed to vary along the thickness direction according to a power-law [13]. Thus, in the laminate coordinate system, the fiber orientation angle at any point along the thickness of the k-th layer of the host FG laminated composite plate can be expressed as

$$\varphi^k(z) = (\varphi_1^k - \varphi_2^k)(f_\lambda^k(z))^r + \varphi_2^k, \quad \lambda = 1 \text{ or } 2$$

$$f_1^k(z) = \frac{z - h_k}{h_{k+1} - h_k} \quad \text{and} \quad f_2^k(z) = \frac{z - h_{k+1}}{h_k - h_{k+1}} \tag{7}$$

where r is the power-law exponent ($0 \leqslant r \leqslant \infty$) and λ is a positive integer. When λ is even, the fiber orientation angle at the bottom surface of the k-th layer of FG laminated composite plate is φ_1^k while that at the top surface of this layer is φ_2^k and the reverse holds for odd values of λ. Thus, the fiber orientation angle at the top surface of the k-th layer of the substrate plate can be modeled as φ_1^k or φ_2^k according as λ equals 1 or 2,

respectively. Now, the elastic matrix for any point in the k-th layer of the substrate FG laminated composite plate can be expressed as

$$[\bar{\mathbf{C}}^k(z)] = [\mathbf{T}^k(z)][\mathbf{C}][\mathbf{T}^k(z)]^{\mathrm{T}}, \quad k = 1, 2, \ldots, N \tag{8}$$

where $[\mathbf{T}^k(z)]$ is the transformation matrix corresponding to the fiber orientation angle $\varphi^k(z)$ at any point (Eq. (7)) in the k-th layer of the host FG laminated composite plate; $[\mathbf{C}]$ is the elastic matrix when fiber orientation angle is 0° with respect to the x-axis of the laminate coordinate system. The constitutive relations of the k-th layer of the substrate FG laminated composite plate can be written as

$$\{\boldsymbol{\sigma}_b^k\} = [\bar{\mathbf{C}}_b^k(z)]\{\boldsymbol{\varepsilon}_b^k\} \quad \text{and} \quad \{\boldsymbol{\sigma}_s^k\} = [\bar{\mathbf{C}}_s^k(z)]\{\boldsymbol{\varepsilon}_s^k\}, \quad k = 1, 2, \ldots, N \tag{9}$$

where $[\bar{\mathbf{C}}_b^k]$ and $[\bar{\mathbf{C}}_s^k]$ are obtained from Eq. (8) as follows:

$$[\bar{\mathbf{C}}_b^k(z)] = \begin{bmatrix} \bar{C}_{11}^k(z) & \bar{C}_{12}^k(z) & \bar{C}_{16}^k(z) \\ \bar{C}_{12}^k(z) & \bar{C}_{22}^k(z) & \bar{C}_{26}^k(z) \\ \bar{C}_{16}^k(z) & \bar{C}_{26}^k(z) & \bar{C}_{66}^k(z) \end{bmatrix} \quad \text{and} \quad [\bar{\mathbf{C}}_s^k(z)] = \begin{bmatrix} \bar{C}_{55}^k(z) & \bar{C}_{45}^k(z) \\ \bar{C}_{45}^k(z) & \bar{C}_{44}^k(z) \end{bmatrix}, \quad k = 1, 2, \ldots, N \tag{10}$$

The constitutive relations for the PFRC material are given by [28,29],

$$\{\boldsymbol{\sigma}_b^k\} = [\bar{\mathbf{C}}_b^k]\{\boldsymbol{\varepsilon}_b^k\} - [\bar{\mathbf{e}}_b]\{\bar{\mathbf{E}}\} \quad \text{and} \quad \{\boldsymbol{\sigma}_s^k\} = [\bar{\mathbf{C}}_s^k]\{\boldsymbol{\varepsilon}_s^k\} - [\bar{\mathbf{e}}_s]\{\bar{\mathbf{E}}\},$$

$$\{\mathbf{D}\} = [\bar{\mathbf{e}}_b]^{\mathrm{T}}\{\boldsymbol{\varepsilon}_b^k\} + [\bar{\mathbf{e}}_s]^{\mathrm{T}}\{\boldsymbol{\varepsilon}_s^k\} + [\bar{\varepsilon}]\{\bar{\mathbf{E}}\} \quad \text{for } k = (N+2) \tag{11}$$

In Eq. (11), the transformed elastic coefficient matrices $[\bar{\mathbf{C}}_b^k]$ and $[\bar{\mathbf{C}}_s^k]$, the transformed piezoelectric coefficient matrices $[\bar{\mathbf{e}}_b]$, $[\bar{\mathbf{e}}_s]$ and the matrix of transformed dielectric constants $[\bar{\varepsilon}]$ referred to the laminate coordinate system (x, y, z) are given by

$$[\bar{\mathbf{C}}_b^k] = \begin{bmatrix} \bar{C}_{11}^k & \bar{C}_{12}^k & \bar{C}_{16}^k \\ \bar{C}_{12}^k & \bar{C}_{22}^k & \bar{C}_{26}^k \\ \bar{C}_{16}^k & \bar{C}_{26}^k & \bar{C}_{66}^k \end{bmatrix}, \quad [\bar{\mathbf{e}}_b] = \begin{bmatrix} 0 & 0 & \bar{e}_{31} \\ 0 & 0 & \bar{e}_{32} \\ 0 & 0 & \bar{e}_{36} \end{bmatrix}, \quad [\bar{\varepsilon}] = \begin{bmatrix} \bar{\varepsilon}_{11} & \bar{\varepsilon}_{12} & 0 \\ \bar{\varepsilon}_{12} & \bar{\varepsilon}_{22} & 0 \\ 0 & 0 & \bar{\varepsilon}_{33} \end{bmatrix}$$

$$[\bar{\mathbf{C}}_s^k] = \begin{bmatrix} \bar{C}_{55}^k & \bar{C}_{45}^k \\ \bar{C}_{45}^k & \bar{C}_{44}^k \end{bmatrix} \quad \text{and} \quad [\bar{\mathbf{e}}_s] = \begin{bmatrix} \bar{e}_{15} & \bar{e}_{25} & 0 \\ \bar{e}_{14} & \bar{e}_{24} & 0 \end{bmatrix}, \quad k = (N+2) \tag{12}$$

The electric field vector $\{\bar{\mathbf{E}}\}$ and the electric displacement vector $\{\mathbf{D}\}$ appearing in Eq. (11) are given by,

$$\{\bar{\mathbf{E}}\} = \{E_x \;\; E_y \;\; E_z\}^{\mathrm{T}} \quad \text{and} \quad \{\mathbf{D}\} = \{D_x \;\; D_y \;\; D_z\}^{\mathrm{T}} \tag{13}$$

in which E_x, E_y and E_z are the electric fields along x-, y- and z-axes, respectively; D_x, D_y and D_z are the corresponding electric displacements. For the problem of our investigation, the electric field is considered to act only along the thickness of the PFRC constraining layer of the ACLD treatment. Thus, recognizing that $E_z = -V/h_p$ with V being the applied voltage difference across the thickness of the PFRC layer, the electric field vector referred to the reference coordinate system can be expressed as

$$\{\bar{\mathbf{E}}\} = \{0 \;\; 0 \;\; -1/h_p\}^{\mathrm{T}} V \tag{14}$$

Using the isothermal stress–strain relation for an isotropic linear viscoelastic material [37], the stress vector $\{\boldsymbol{\sigma}_s^k\}$ $(k = N+1)$ for the viscoelastic damping material layer can be written as

$$\{\boldsymbol{\sigma}_s^k\} = G(t)[\mathbf{C}_{ss}^k]\{\boldsymbol{\varepsilon}_s^k(0)\} + \int_0^t G(t-\tau)[\mathbf{C}_{ss}^k]\frac{\partial}{\partial\tau}\{\boldsymbol{\varepsilon}_s^k(\tau)\}\,\mathrm{d}\tau \quad \text{for } k = (N+1) \tag{15}$$

where $G(t)$ is the material relaxation function and the strain vector $\{\boldsymbol{\varepsilon}_s^k(t)\}$ is restricted to zero for $t \in (-\infty, 0)$ and the matrix $[\mathbf{C}_{ss}^k]$ is a (2×2) unit matrix. It is known that the transverse shear deformations of the viscoelastic layer are attributed to the constrained layer damping of the host structure. Also, the extensional

stiffness of the viscoelastic constrained layer is very small as compared to the host FG laminated composite plate and the piezoelectric composite constraining layer. Thus, the extensional counterpart of the strain energy for the viscoelastic layer may be neglected in the estimation of the total potential energy of the overall plate. The first variation of the total potential energy T_P and the kinetic energy T_K of the host FG laminated composite plate integrated with a patch of ACLD treatment can be written as [38]

$$\delta T_P = \frac{1}{2}\int_0^a \int_0^b \left[\sum_{\substack{k=1 \\ k\neq N+1}}^{N+2} \int_{h_k}^{h_{k+1}} \{\delta\boldsymbol{\varepsilon}_b^k\}^{\mathrm{T}}\{\boldsymbol{\sigma}_b^k\}\,\mathrm{d}z + \sum_{k=1}^{N+2} \int_{h_k}^{h_{k+1}} \{\delta\boldsymbol{\varepsilon}_s^k\}^{\mathrm{T}}\{\boldsymbol{\sigma}_s^k\}\,\mathrm{d}z - \int_{h_k}^{h_{k+1}} \{\delta\bar{\mathbf{E}}\}^{\mathrm{T}}\{\mathbf{D}\}\Big|_{k=N+2}\,\mathrm{d}z - 2p\delta w \right] \mathrm{d}x\,\mathrm{d}y \tag{16}$$

$$\delta T_K = \frac{1}{2}\int_0^a \int_0^b \left[\sum_{k=1}^{N+2} \int_{h_k}^{h_{k+1}} (\rho^k \{\delta\dot{\mathbf{d}}_t\}^{\mathrm{T}}\{\dot{\mathbf{d}}_t\})\,\mathrm{d}z \right] \mathrm{d}x\,\mathrm{d}y \tag{17}$$

where $p(x, y, t)$ is a uniformly distributed transverse step load and ρ^k is the mass density of the k-th layer of the overall laminated plate. Since the overall plate is very thin, the rotary inertia of the overall plate may be neglected and hence, the rotational velocities are not considered to estimate the kinetic energy of the overall plate. The overall plate is discretized by the eight-noded isoparametric quadrilateral element. Thus, the generalized displacement vectors at any point within the element can be written as

$$\{\mathbf{d}_t\} = [\mathbf{N}_t]\{\mathbf{d}_t^e\} \quad \text{and} \quad \{\mathbf{d}_r\} = [\mathbf{N}_r]\{\mathbf{d}_r^e\} \tag{18}$$

where $\{\mathbf{d}_t^e\}$ and $\{\mathbf{d}_r^e\}$ are the nodal generalized translational and rotational displacement vector, respectively; and the matrices $[\mathbf{N}_t]$ and $[\mathbf{N}_r]$ are the shape function matrices. The equations of motion are derived by employing the extended Hamilton's principle for the nonconservative system [39]:

$$\int_{t_1}^{t_2} (\delta T_k - \delta T_p)\,\mathrm{d}t = 0 \tag{19}$$

Substituting Eqs. (16) and (17) into Eq. (19) and then using Eqs. (9), (11), (15), (5) and (18), the nonlinear governing equations of motion for a typical element of the substrate FG laminated composite plate integrated with the ACLD treatment can be derived as

$$\begin{aligned}
&[\mathbf{M}]^e\{\ddot{\mathbf{d}}_t^e\} + [\mathbf{K}_{tt}]^e\{\mathbf{d}_t^e\} + [\mathbf{K}_{tr}]^e\{\mathbf{d}_r^e\} + [\mathbf{K}_{tt}^v]^e\left(G(t)\{\mathbf{d}_t^e(0)\} + \int_0^t \left[G(t-\tau)\frac{\partial}{\partial\tau}\{\mathbf{d}_t^e(\tau)\}\right]\mathrm{d}\tau\right) \\
&+ [\mathbf{K}_{tr}^v]^e\left(G(t)\{\mathbf{d}_r^e(0)\} + \int_0^t \left[G(t-\tau)\frac{\partial}{\partial\tau}\{\mathbf{d}_r^e(\tau)\}\right]\mathrm{d}\tau\right) = \{\mathbf{F}_{et}\}^e V + \{\mathbf{F}_m\}^e
\end{aligned} \tag{20}$$

$$\begin{aligned}
&[\mathbf{K}_{rt}]^e\{\mathbf{d}_t^e\} + [\mathbf{K}_{rr}]^e\{\mathbf{d}_r^e\} + [\mathbf{K}_{rt}^v]^e\left(G(t)\{\mathbf{d}_t^e(0)\} + \int_0^t \left[G(t-\tau)\frac{\partial}{\partial\tau}\{\mathbf{d}_t^e(\tau)\}\right]\mathrm{d}\tau\right) \\
&+ [\mathbf{K}_{rr}^v]^e\left(G(t)\{\mathbf{d}_r^e(0)\} + \int_0^t \left[G(t-\tau)\frac{\partial}{\partial\tau}\{\mathbf{d}_r^e(\tau)\}\right]\mathrm{d}\tau\right) = \{\mathbf{F}_{er}\}^e V
\end{aligned} \tag{21}$$

wherein, the elemental stiffness matrices ($[\mathbf{K}_{tt}]^e, [\mathbf{K}_{tr}]^e, [\mathbf{K}_{rt}]^e, [\mathbf{K}_{rr}]^e, [\mathbf{K}_{tt}^v]^e, [\mathbf{K}_{tr}^v]^e, [\mathbf{K}_{rt}^v]^e$ and $[\mathbf{K}_{rr}^v]^e$), the elemental mass matrix ($[\mathbf{M}]^e$), the elemental electro-elastic coupling vectors ($[\mathbf{F}_{et}]^e, [\mathbf{F}_{er}]^e$) and the mechanical load vector $\{\mathbf{F}_m\}^e$ are given by

$$[\mathbf{K}_{tt}]^e = \int_0^{a_e}\int_0^{b_e} ([\mathbf{B}_{b\alpha t}]^{\mathrm{T}}[\mathbf{A}_b^{sp}][\mathbf{B}_{bt}] + [\mathbf{B}_{st}]^{\mathrm{T}}[\mathbf{A}_s^{sp}][\mathbf{B}_{st}])\,\mathrm{d}x\,\mathrm{d}y, \quad [\mathbf{K}_{tt}^v]^e = \int_0^{a_e}\int_0^{b_e} [\mathbf{B}_{st}]^{\mathrm{T}}[\mathbf{A}_s^v][\mathbf{B}_{st}]\,\mathrm{d}x\,\mathrm{d}y,$$

$$[\mathbf{K}_{tr}]^e = \int_0^{a_e}\int_0^{b_e} ([\mathbf{B}_{b\alpha t}]^{\mathrm{T}}[\mathbf{B}_b^{sp}][\mathbf{B}_{br}] + [\mathbf{B}_{st}]^{\mathrm{T}}[\mathbf{B}_s^{sp}][\mathbf{B}_{sr}])\,\mathrm{d}x\,\mathrm{d}y, \quad [\mathbf{K}_{tr}^v]^e = \int_0^{a_e}\int_0^{b_e} [\mathbf{B}_{st}]^{\mathrm{T}}[\mathbf{B}_s^v][\mathbf{B}_{sr}]\,\mathrm{d}x\,\mathrm{d}y,$$

$$[\mathbf{K}_{rt}]^e = \int_0^{a_e}\int_0^{b_e} ([\mathbf{B}_{br}]^{\mathrm{T}}[\mathbf{S}_b^{sp}][\mathbf{B}_{bt}] + [\mathbf{B}_{sr}]^{\mathrm{T}}[\mathbf{S}_s^{sp}][\mathbf{B}_{st}])\,\mathrm{d}x\,\mathrm{d}y, \quad [\mathbf{K}_{rt}^v]^e = \int_0^{a_e}\int_0^{b_e} [\mathbf{B}_{sr}]^{\mathrm{T}}[\mathbf{S}_s^v][\mathbf{B}_{st}]\,\mathrm{d}x\,\mathrm{d}y,$$

$$[\mathbf{K}_{rr}]^e = \int_0^{a_e}\int_0^{b_e}([\mathbf{B}_{br}]^{\mathrm{T}}[\mathbf{D}_b^{sp}][\mathbf{B}_{br}] + [\mathbf{B}_{sr}]^{\mathrm{T}}[\mathbf{D}_s^{sp}][\mathbf{B}_{sr}])\,\mathrm{d}x\,\mathrm{d}y, \quad [\mathbf{K}_{rr}^{v}]^e = \int_0^{a_e}\int_0^{b_e}[\mathbf{B}_{sr}]^{\mathrm{T}}[\mathbf{D}_s^{v}][\mathbf{B}_{sr}]\,\mathrm{d}x\,\mathrm{d}y,$$

$$\{\mathbf{F}_{et}\}^e = \int_0^{a_e}\int_0^{b_e}([\mathbf{B}_{b\alpha t}]^{\mathrm{T}}[\mathbf{A}_{be}] + [\mathbf{B}_{st}]^{\mathrm{T}}[\mathbf{A}_{se}])\,\mathrm{d}x\,\mathrm{d}y, \quad \{\mathbf{F}_{er}\}^e = \int_0^{a_e}\int_0^{b_e}([\mathbf{B}_{br}]^{\mathrm{T}}[\mathbf{B}_{be}] + [\mathbf{B}_{sr}]^{\mathrm{T}}[\mathbf{B}_{se}])\,\mathrm{d}x\,\mathrm{d}y,$$

$$[\mathbf{M}]^e = \int_0^{a^e}\int_0^{b^e} I\bar{m}[\mathbf{N}_t]^{\mathrm{T}}[\mathbf{N}_t]\,\mathrm{d}x\,\mathrm{d}y, \quad \{\mathbf{F}_m\}^e = \int_0^{a_e}\int_0^{b_e}[\mathbf{N}_t]^{\mathrm{T}}\{\mathbf{f}\}\mathrm{d}x\,\mathrm{d}y \tag{22}$$

In Eq. (22), a^e and b^e are the length and the width of an element in consideration while the various strain–nodal displacement matrices, the rigidity matrices, the mass parameter ($I\bar{m}$) and the load vector ($\{\mathbf{f}\}$) are as follows,

$$([\mathbf{B}_{bt}],[\mathbf{B}_{b\alpha t}],[\mathbf{B}_{st}]) = ([\mathbf{L}_{bt}],[\mathbf{L}_{b\alpha t}],[\mathbf{L}_{st}])[\mathbf{N}_t], \quad ([\mathbf{B}_{br}],[\mathbf{B}_{sr}]) = ([\mathbf{L}_{br}],[\mathbf{L}_{sr}])[\mathbf{N}_r],$$

$$([\mathbf{A}_b^{sp}],[\mathbf{B}_b^{sp}]) = \sum_{\substack{k=1\\k\neq N+1}}^{N+2}\int_{h_k}^{h_{k+1}}[\bar{\mathbf{C}}_b^k](1,[\mathbf{Z}_b^k])\,\mathrm{d}z, \quad ([\mathbf{A}_s^{v}],[\mathbf{B}_s^{v}]) = \int_{h_k}^{h_{k+1}}[\mathbf{C}_s^k](1,[\mathbf{Z}_s^k])|_{k=N+1}\,\mathrm{d}z,$$

$$([\mathbf{S}_b^{sp}],[\mathbf{D}_b^{sp}]) = \sum_{\substack{k=1\\k\neq N+1}}^{N+2}\int_{h_k}^{h_{k+1}}[\mathbf{Z}_b^k]^{\mathrm{T}}[\bar{\mathbf{C}}_b^k](1,[\mathbf{Z}_b^k])\,\mathrm{d}z, \quad ([\mathbf{A}_s^{sp}],[\mathbf{B}_s^{sp}]) = \sum_{\substack{k=1\\k\neq N+1}}^{N+2}\int_{h_k}^{h_{k+1}}[\bar{\mathbf{C}}_s^k](1,[\mathbf{Z}_s^k])\,\mathrm{d}z,$$

$$([\mathbf{S}_s^{sp}],[\mathbf{D}_s^{sp}]) = \sum_{\substack{k=1\\k\neq N+1}}^{N+2}\int_{h_k}^{h_{k+1}}[\mathbf{Z}_s^k]^{\mathrm{T}}[\bar{\mathbf{C}}_s^k](1,[\mathbf{Z}_s^k])\,\mathrm{d}z, \quad ([\mathbf{S}_s^{v}],[\mathbf{D}_s^{v}]) = \int_{h_k}^{h_{k+1}}[\mathbf{Z}_s^k]^{\mathrm{T}}[\mathbf{C}_s^k](1,[\mathbf{Z}_s^k])|_{k=N+1}\,\mathrm{d}z,$$

$$([\mathbf{A}_{be}],[\mathbf{B}_{be}]) = \int_{h_k}^{h_{k+1}}(1,[\mathbf{Z}_b^k]^{\mathrm{T}})[\bar{\mathbf{e}}_b]\{0\ \ 0\ \ -1/h_p\}^{\mathrm{T}}|_{k=N+2}\,\mathrm{d}z, \quad \{\mathbf{f}\} = [0\ \ 0\ \ p]^{\mathrm{T}},$$

$$([\mathbf{A}_{se}],[\mathbf{B}_{se}]) = \int_{h_k}^{h_{k+1}}(1,[\mathbf{Z}_s^k]^{\mathrm{T}})[\bar{\mathbf{e}}_s]\{0\ \ 0\ \ -1/h_p\}^{\mathrm{T}}|_{k=N+2}\,\mathrm{d}z, \quad I\bar{m} = \sum_{k=1}^{N+2}\int_{h_k}^{h_{k+1}}\rho^k\,\mathrm{d}z \tag{23}$$

It is to be noted that for an element without integrated with the ACLD treatment, the electro-elastic coupling vectors become null vectors. In the above formulation, the bending and shear counterparts of the stiffness matrices are formulated separately and computed by the application of selective integration scheme in a straightforward manner. In the feed back control strategy, the control voltage supplied to the ACLD patch can be expressed in terms of the velocities of the global nodal dof as follows:

$$V = -k_d\dot{w} = -k_d[\mathbf{U}]\{\dot{\mathbf{X}}_t\} \tag{24}$$

in which k_d is the velocity feed back control gain, $[\mathbf{U}]$ is a row matrix defining the location of sensing the velocity signal that will be fed back to the patch and $\{\mathbf{X}_t\}$ is the global nodal translational dof. Assembling the elemental governing equations, given by Eqs. (20) and (21), in the global space and then using Eq. (24), the following nonlinear closed-loop governing equations of motion for the substrate FG laminated composite plates activated by the ACLD treatment can be obtained:

$$\begin{aligned}[\mathbf{M}]\{\ddot{\mathbf{X}}_t\} + [\mathbf{C}_{tt}]\{\dot{\mathbf{X}}_t\} + [\mathbf{K}_{tt}]\{\mathbf{X}_t\} + [\mathbf{K}_{tr}]\{\mathbf{X}_r\} + [\mathbf{K}_{tt}^{v}]\left(G(t)\{\mathbf{X}_t(0)\} + \int_0^t\left[G(t-\tau)\frac{\partial}{\partial\tau}\{\mathbf{X}_t(\tau)\}\right]\mathrm{d}\tau\right)\\ + [\mathbf{K}_{tr}^{v}]\left(G(t)\{\mathbf{X}_r(0)\} + \int_0^t\left[G(t-\tau)\frac{\partial}{\partial\tau}\{\mathbf{X}_r(\tau)\}\right]\mathrm{d}\tau\right) = \{\mathbf{F}_m\}\end{aligned} \tag{25}$$

$$[\mathbf{C}_{rt}]\{\dot{\mathbf{X}}_t\} + [\mathbf{K}_{rt}]\{\mathbf{X}_t\} + [\mathbf{K}_{rr}]\{\mathbf{X}_r\} + [\mathbf{K}^v_{rt}]\left(G(t)\{\mathbf{X}_t(0)\} + \int_0^t \left[G(t-\tau)\frac{\partial}{\partial\tau}\{\mathbf{X}_t(\tau)\}\right]\mathrm{d}\tau\right)$$
$$+ [\mathbf{K}^v_{rr}]\left(G(t)\{\mathbf{X}_r(0)\} + \int_0^t \left[G(t-\tau)\frac{\partial}{\partial\tau}\{\mathbf{X}_r(\tau)\}\right]\mathrm{d}\tau\right) = 0 \tag{26}$$

where $[\mathbf{C}_{tt}] = k_d\{\mathbf{F}_{et}\}[\mathbf{N}]$, $[\mathbf{C}_{rt}] = k_d\{\mathbf{F}_{er}\}[\mathbf{N}]$; $[\mathbf{K}_{tt}], [\mathbf{K}_{tr}], [\mathbf{K}_{rt}], [\mathbf{K}_{rr}], [\mathbf{K}^v_{tt}], [\mathbf{K}^v_{tr}], [\mathbf{K}^v_{rt}]$ and $[\mathbf{K}^v_{rr}]$ are the global stiffness matrices, $[\mathbf{M}]$ is the global mass matrix, $\{\mathbf{X}_r\}$ is the global nodal generalized rotational displacement vector, $\{\mathbf{F}_m\}$ is the global nodal mechanical force vector, $\{\mathbf{F}_{et}\}$ and $\{\mathbf{F}_{er}\}$ are the global electro-elastic coupling vectors.

In the Laplace domain, the function $s\tilde{G}(s)$ is referred to as the material modulus function [34] with $\tilde{G}(s)$ being the Laplace transform of material relaxation function $G(t)$ of the viscoelastic material. According to the Golla–Hughes–McTavish (GHM) method for modeling the viscoelastic material in time domain, this modulus function is represented by a series of mini-oscillator terms as follows [34]:

$$s\tilde{G}(s) = G^\infty\left[1 + \sum_{q=1}^{R}\alpha_q\frac{s^2 + 2\hat{\xi}_q\hat{\omega}_q s}{s^2 + 2\hat{\xi}_q\hat{\omega}_q s + \hat{\omega}_q^2}\right] \tag{27}$$

where G^∞ corresponds to the equilibrium value of the modulus i.e. the final value of $G(t)$. Each mini-oscillator term is a second-order rational function involving three positive constants $\alpha_q, \hat{\xi}_q$ and $\hat{\omega}_q$. These constants govern the shape of the modulus function in the complex s-domain [34]. Now considering a GHM material modulus function with one mini-oscillator term [34], i.e.,

$$s\tilde{G}(s) = G^\infty\left[1 + \alpha\frac{s^2 + 2\hat{\xi}\hat{\omega}s}{s^2 + 2\hat{\xi}\hat{\omega}s + \hat{\omega}^2}\right] \tag{28}$$

the auxiliary dissipation coordinates $\{\mathbf{z}_t\}$, $\{\mathbf{z}_r\}$ are introduced as follows [34]:

$$\{\tilde{\mathbf{z}}_t(s)\} = \frac{\hat{\omega}^2}{s^2 + 2\hat{\xi}\hat{\omega}s + \hat{\omega}^2}\{\tilde{\mathbf{X}}_t(s)\} \quad \text{and} \quad \{\tilde{\mathbf{z}}_r(s)\} = \frac{\hat{\omega}^2}{s^2 + 2\hat{\xi}\hat{\omega}s + \hat{\omega}^2}\{\tilde{\mathbf{X}}_r(s)\} \tag{29}$$

where $\{\tilde{\mathbf{z}}_t(s)\}$ and $\{\tilde{\mathbf{z}}_r(s)\}$ are the Laplace transforms of $\{\mathbf{z}_t\}$ and $\{\mathbf{z}_r\}$, respectively. Taking inverse Laplace transform of Eq. (29), the time domain representation of auxiliary dissipation coordinates can be written as

$$\{\ddot{\mathbf{z}}_t\} + 2\hat{\omega}\hat{\xi}\{\dot{\mathbf{z}}_t\} + \hat{\omega}^2\{\mathbf{z}_t\} - \hat{\omega}^2\{\mathbf{X}_t\} = 0 \tag{30}$$

$$\{\ddot{\mathbf{z}}_r\} + 2\hat{\omega}\hat{\xi}\{\dot{\mathbf{z}}_r\} + \hat{\omega}^2\{\mathbf{z}_r\} - \hat{\omega}^2\{\mathbf{X}_r\} = 0 \tag{31}$$

Making use of Eqs. (28) and (29) in the Laplace transform of Eqs. (25) and (26) and subsequently, taking inverse Laplace transform of the resulting equations, the following global equations of motion are obtained:

$$[\mathbf{M}]\{\ddot{\mathbf{X}}_t\} + [\mathbf{C}_{tt}]\{\dot{\mathbf{X}}_t\} + [\mathbf{K}^c_{tt}]\{\mathbf{X}_t\} + [\mathbf{K}^c_{tr}]\{\mathbf{X}_r\} + [\mathbf{K}^d_{tt}]\{\mathbf{z}_t\} + [\mathbf{K}^d_{tr}]\{\mathbf{z}_r\} = \{\mathbf{F}_m\} \tag{32}$$

$$[\mathbf{C}_{rt}]\{\dot{\mathbf{X}}_t\} + [\mathbf{K}^c_{rt}]\{\mathbf{X}_t\} + [\mathbf{K}^c_{rr}]\{\mathbf{X}_r\} + [\mathbf{K}^d_{rt}]\{\mathbf{z}_t\} + [\mathbf{K}^d_{rr}]\{\mathbf{z}_r\} = 0 \tag{33}$$

in which

$$[\mathbf{K}^c_{tt}] = [\mathbf{K}_{tt}] + [\mathbf{K}^v_{tt}]G^\infty(1+\alpha), \quad [\mathbf{K}^c_{tr}] = [\mathbf{K}_{tr}] + [\mathbf{K}^v_{tr}]G^\infty(1+\alpha), \quad [\mathbf{K}^d_{tt}] = -[\mathbf{K}^v_{tt}]G^\infty\alpha,$$

$$[\mathbf{K}^d_{tr}] = -[\mathbf{K}^v_{tr}]G^\infty\alpha, \quad [\mathbf{K}^c_{rt}] = [\mathbf{K}_{rt}] + [\mathbf{K}^v_{rt}]G^\infty(1+\alpha), \quad [\mathbf{K}^c_{rr}] = [\mathbf{K}_{rr}] + [\mathbf{K}^v_{rr}]G^\infty(1+\alpha),$$

$$[\mathbf{K}^d_{rt}] = -[\mathbf{K}^v_{rt}]G^\infty\alpha, \quad [\mathbf{K}^d_{rr}] = -[\mathbf{K}^v_{rr}]G^\infty\alpha \tag{34}$$

After imposing the boundary conditions, the global rotational dof $\{\mathbf{X}_r\}$ can be condensed from Eqs. (30)–(32) to obtain the following final global closed-loop equations of motion in terms of the global nodal translational dofs ($\{\mathbf{X}_t\}$) and the dissipative coordinates ($\{\mathbf{z}_t\}, \{\mathbf{z}_r\}$) as follows:

$$[\bar{\mathbf{M}}]\{\ddot{\mathbf{X}}(t)\} + [\bar{\mathbf{C}}]\{\dot{\mathbf{X}}(t)\} + [\bar{\mathbf{K}}]\{\mathbf{X}(t)\} = \{\bar{\mathbf{F}}\} \tag{35}$$

where

$$[\bar{\mathbf{M}}]=\begin{bmatrix}[\mathbf{M}] & [\tilde{\mathbf{O}}_{tt}] & [\tilde{\mathbf{O}}_{tr}]\\ [\tilde{\mathbf{O}}_{tt}] & [\mathbf{I}_{tt}] & [\tilde{\mathbf{O}}_{tr}]\\ [\tilde{\mathbf{O}}_{rt}] & [\tilde{\mathbf{O}}_{rt}] & [\mathbf{I}_{rr}]\end{bmatrix},\quad [\bar{\mathbf{C}}]=\begin{bmatrix}[\mathbf{C}_{tt}^{1}] & [\tilde{\mathbf{O}}_{tt}] & [\tilde{\mathbf{O}}_{tr}]\\ [\tilde{\mathbf{O}}_{tt}] & [\mathbf{C}_{tt}^{z2}] & [\tilde{\mathbf{O}}_{tr}]\\ [\mathbf{C}_{rt}^{3}] & [\tilde{\mathbf{O}}_{rt}] & [\mathbf{C}_{rr}^{z3}]\end{bmatrix},\quad [\bar{\mathbf{K}}]=\begin{bmatrix}[\mathbf{K}_{tt}^{1}] & [\mathbf{K}_{tt}^{z1}] & [\mathbf{K}_{tr}^{z1}]\\ [\mathbf{K}_{tt}^{2}] & [\mathbf{K}_{tt}^{z2}] & [\tilde{\mathbf{O}}_{tr}]\\ [\mathbf{K}_{rt}^{3}] & [\mathbf{K}_{rt}^{z3}] & [\mathbf{K}_{rr}^{z3}]\end{bmatrix}$$

$$\{\bar{\mathbf{F}}\}=[\{F_m\}^{\mathrm{T}}\quad\{\tilde{\mathbf{O}}_t\}^{\mathrm{T}}\quad\{\tilde{O}_r\}^{\mathrm{T}}]^{\mathrm{T}},\quad \{\mathbf{X}(t)\}=[\{X_t(t)\}^{\mathrm{T}}\ \{z_t(t)\}^{\mathrm{T}}\ \{z_r(t)\}^{\mathrm{T}}]^{\mathrm{T}}$$

$$[\mathbf{C}_{tt}^{1}]=[\mathbf{C}_{tt}]-[\mathbf{K}_{tr}^{c}][\mathbf{K}_{rr}^{c}]^{-1}[\mathbf{C}_{rt}],\quad [\mathbf{K}_{tt}^{1}]=[\mathbf{K}_{tt}^{c}]-[\mathbf{K}_{tr}^{c}][\mathbf{K}_{rr}^{c}]^{-1}[\mathbf{K}_{rt}^{c}]$$

$$[\mathbf{K}_{tt}^{z1}]=[\mathbf{K}_{tt}^{d}]-[\mathbf{K}_{tr}^{c}][\mathbf{K}_{rr}^{c}]^{-1}[\mathbf{K}_{rt}^{d}],\quad [\mathbf{K}_{tr}^{z1}]=[\mathbf{K}_{tr}^{d}]-[\mathbf{K}_{tr}^{c}][\mathbf{K}_{rr}^{c}]^{-1}[\mathbf{K}_{rr}^{d}]$$

$$[\mathbf{C}_{tt}^{z2}]=I_{tt}(2\hat{\omega}\hat{\xi}),\quad [\mathbf{K}_{tt}^{2}]=-I_{tt}\hat{\omega}^2,\quad [\mathbf{K}_{tt}^{z2}]=I_{tt}\hat{\omega}^2$$

$$[\mathbf{C}_{rt}^{3}]=\hat{\omega}^2[\mathbf{K}_{rr}^{c}]^{-1}[\mathbf{C}_{rt}],\quad [\mathbf{C}_{rr}^{z3}]=I_{rr}(2\hat{\omega}\hat{\xi}),\quad [\mathbf{K}_{rt}^{3}]=\hat{\omega}^2[\mathbf{K}_{rr}^{c}]^{-1}[\mathbf{K}_{rt}^{c}]$$

$$[\mathbf{K}_{rt}^{z3}]=\hat{\omega}^2[\mathbf{K}_{rr}^{c}]^{-1}[\mathbf{K}_{rt}^{d}],\quad [\mathbf{K}_{rr}^{z3}]=I_{rr}\hat{\omega}^2+\hat{\omega}^2[\mathbf{K}_{rr}^{c}]^{-1}[\mathbf{K}_{rr}^{d}],\tag{36}$$

wherein, $[\tilde{\mathbf{O}}_{tt}]$, $[\tilde{\mathbf{O}}_{tr}]$, $[\tilde{\mathbf{O}}_{rt}]$, $[\tilde{\mathbf{O}}_{t}]$ and $[\tilde{\mathbf{O}}_{r}]$ are null matrices and null vectors with the same order of $[\mathbf{K}_{tt}]$, $[\mathbf{K}_{tr}]$, $[\mathbf{K}_{rt}]$, $\{\mathbf{z}_t(t)\}$ and $\{\mathbf{z}_r(t)\}$, respectively.

3. Numerical results and discussions

In order to investigate the performance of the PFRC material as the constraining layer of the ACLD treatment for controlling the nonlinear forced vibrations of the FG laminated composite plates, square symmetric and asymmetric FG laminated composite plates integrated with a square patch of the ACLD treatment (Fig. 1) are considered for evaluating the numerical results. The patch of the ACLD treatment is placed at the center of the substrate plate as shown in Fig. 1. The control voltage across the thickness of the PFRC constraining layer of the ACLD patch is negatively proportional to the velocity of the mid-point ($a/2$, $b/2$, $h/2$) of the substrate plate. The side-to-thickness ratio ($s=a/h$) of the square substrate FG laminated composite plates is considered as 100 with the thickness of the plates being 4 mm. Unless otherwise mentioned, the thickness of the viscoelastic layer and the PFRC layer of the ACLD patch are considered as 50 and 250 μm, respectively. Also, unless otherwise stated, the fiber orientation angle in the PFRC constraining layer is 0° and the applied uniformly distributed step load acts vertically upward. The material properties of the unidirectional fiber reinforced composite in which the fiber orientation angle is 0° with respect to the x-axis are considered as [40]

$$E_{11}=36.2\,\mathrm{GPa},\quad E_{22}=10.6\,\mathrm{GPa},\quad G_{12}=5.6\,\mathrm{GPa},\quad G_{13}=3.6\,\mathrm{GPa},$$

$$G_{23}=3.2\,\mathrm{GPa},\quad v_{12}=0.26,\quad \rho=1870\,\mathrm{kg/m^3}$$

Thus, using Eqs. (7) and (8) the elastic properties $[\bar{\mathbf{C}}^{k}(z)]$ at any point in the k-the layer of the host FG laminated composite plate can be computed after knowing the elastic matrix $[\mathbf{C}]$ from the above material properties. The material properties of the viscoelastic layer in terms of the GHM parameters are considered as [27]

$$G^{\infty}=3.887\times10^{4}\,\mathrm{N/m^2},\quad \alpha_1=2.3263\times10^{4},\quad \alpha_2=4.1977\times10^{1},\quad \alpha_3=3.5174\times10^{1},$$

$$\hat{\omega}_1=6.6169\times10^{6},\quad \hat{\omega}_2=3.2854\times10^{4},\quad \hat{\omega}_3=4.7515\times10^{4},\quad \hat{\xi}_1=3.0787,$$

$$\hat{\xi}_2=1.4288\times10^{2},\quad \hat{\xi}_3=6.1785\times10^{2},\quad \rho=789.5\,\mathrm{kg/m^3}$$

The PZT5H/epoxy composite with 40% fiber volume fraction is considered as the material of the active constraining layer and its effective elastic and piezoelectric coefficients are obtained from the micromechanics

model [28] as follows:

$$C_{11} = 32.6\,\text{GPa}, \quad C_{12} = 4.3\,\text{GPa}, \quad C_{22} = 7.2\,\text{GPa}, \quad C_{44} = 1.05\,\text{GPa}, \quad C_{55} = C_{66} = 1.29\,\text{GPa},$$

$$e_{31} = -6.76\,\text{C/m}^2, \quad e_{32} = -0.076\,\text{C/m}^2, \quad \rho = 3640\,\text{kg/m}^3$$

The following simply supported boundary conditions are used to evaluate the numerical results:

$$v_0 = w_0 = \theta_y = 0 \quad \text{at } x = 0, a \quad \text{and} \quad u_0 = w_0 = \theta_x = 0 \quad \text{at } y = 0, b$$

The following non-dimensional quantities are used for presenting the results.

$$Q = \frac{ps^4}{E_2}, \quad \bar{\sigma}_x = \frac{\sigma_x s^2}{E_2}, \quad \bar{\sigma}_y = \frac{\sigma_y s^2}{E_2}$$

Two types of FG laminated composite plates considered as the substrates for the numerical examples are described as follows:

FG laminate 1: This FG laminated substrate plate is a symmetric square plate constructed by laminating two orthotropic FG layers such that the top and bottom surfaces of the plate have 0° fiber orientation angle while the fiber orientation angle at the interface between the layers is 90° as shown in Fig. 3(a). The fiber orientation angle in each FG layer of the plate varies from 0° to 90° according to Eq. (7) as shown in Fig. 3(b). The continuity of material properties of this FG laminate across its thickness can be observed from Fig. 3(c).

FG laminate 2: This FG laminated substrate plate is an asymmetric square plate constructed by laminating three orthotropic FG layers such that the fiber orientation angle at the top and bottom surfaces of the plate are 0° and 90°, respectively, as shown in Fig. 4(a). The fiber orientation angle at the interface between layers 1

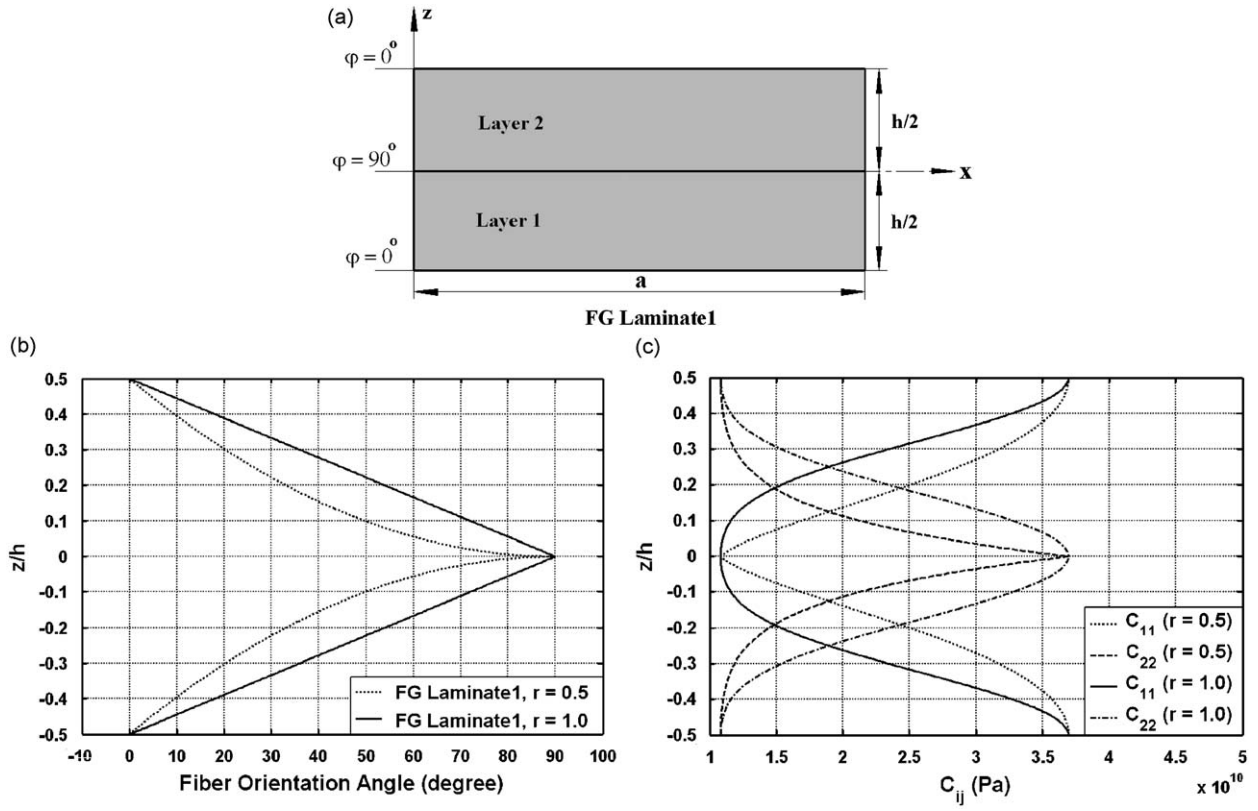

Fig. 3. (a) Symmetric two layered FG laminated composite plate (FG laminate 1, $a/h = 100$, $a = b$), (b) variation of the fiber orientation angle (φ) and (c) the elastic properties (C_{ij}) along the thickness direction of the FG laminate 1.

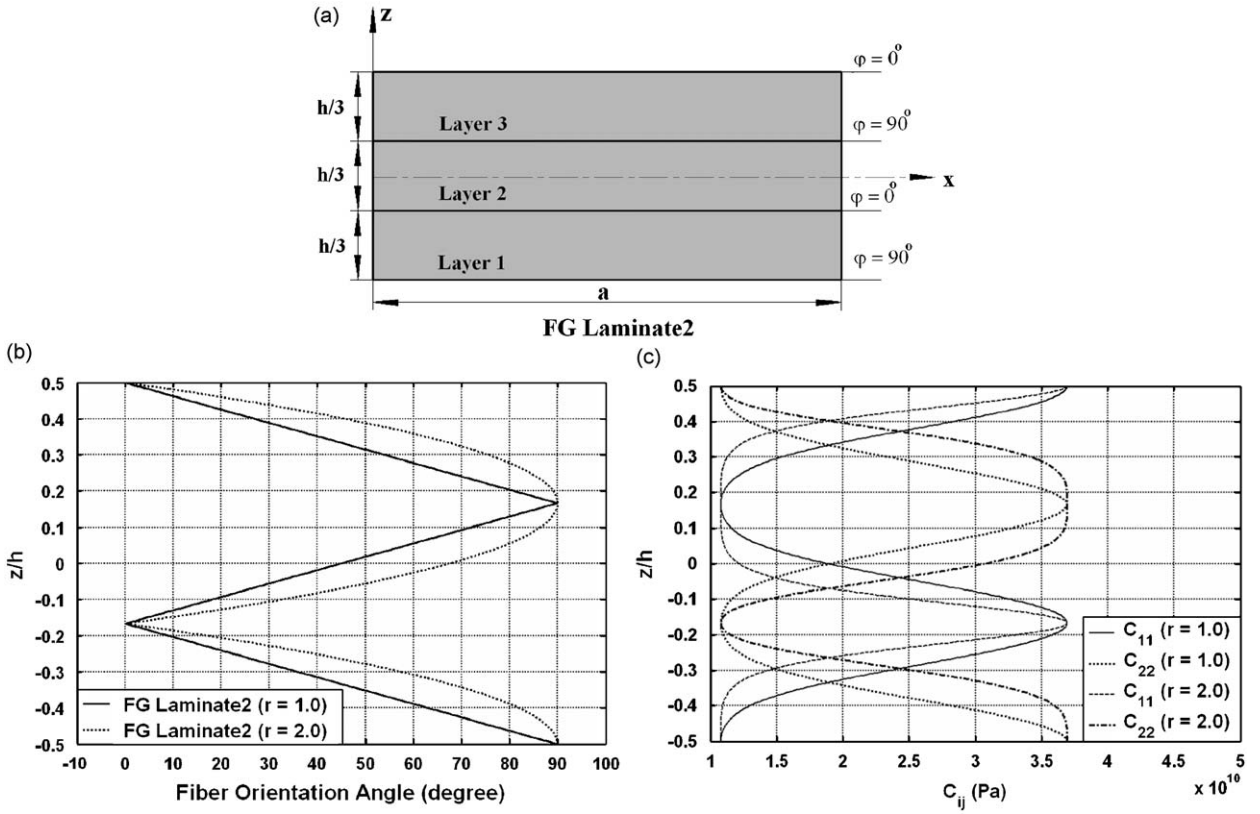

Fig. 4. (a) Asymmetric three layered FG laminated composite plate (FG laminate 2, $a/h = 100$, $a = b$), (b) variation of the fiber orientation angle (φ) and (c) the elastic properties (C_{ij}) along the thickness direction of the FG laminate 2.

and 2 is 0° while that between layers 2 and 3 is 90°. Fig. 4(b) illustrates the variation of the fiber orientation angle according to Eq. (7) in each FG layer of the plate. Fig. 4(c) displays that the elastic properties of this laminate varies continuously across its thickness.

In order to verify the continuity of the stresses across the thickness of the substrate FG laminated composite plates as described above, the static responses of the laminates without integrated with the ACLD patch are first studied. The static response of the FG laminate 1 are compared with that of a conventional symmetric laminated composite plate (0°/90°/0°) whose thickness (h) and side-to-thickness ratio ($s = a/h$) are identical to those of this FG laminated plate. Fig. 5(a) illustrates the variation of dimensionless nonlinear center deflection of the FG laminated composite plate with the dimensionless intensity of the uniformly distributed load. It may be observed from this figure that the nonlinear center deflections of the FG laminated composite plate do not differ significantly for different values of power-law index r. Also, the center deflections are almost indistinguishable from those of the laminated composite plate (0°/90°/0°) when the value of power-law index r equals 0.2. For a particular mechanical load having the numerical value as 2000 N/m^2, Figs. 5(b) and (c) illustrate the distributions of the dimensionless in-plane normal stresses ($\bar{\sigma}_x, \bar{\sigma}_y$) across the thickness of this symmetric FG laminated composite plate. It may be observed from these figures that unlike the discontinuous stresses across the thickness of the laminated composite plate (0°/90°/0°), the stresses across the thickness of the FG laminated composite plate are smooth and continuous. Similar static responses of the FG laminate 2 are demonstrated in Fig. 6 indicating the continuity of stresses across its thickness.

So far, no literature is available for comparing the results for the problem being analyzed in this paper. Hence, to verify the implementation of the GHM method, the linear dynamic responses of the simply supported two-layered FG laminated composite plate shown in Fig. 3(a) are computed in the frequency

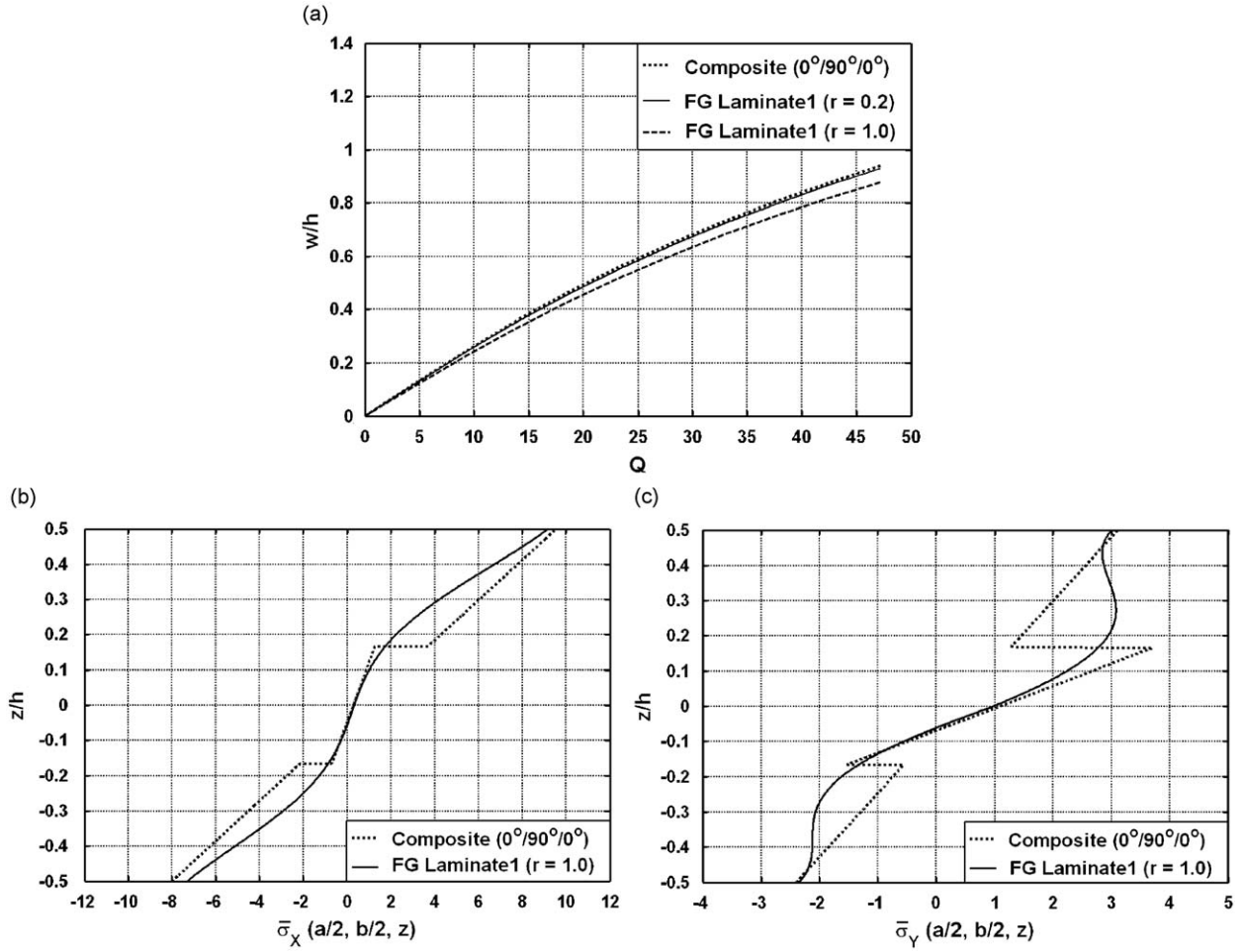

Fig. 5. (a) Variation of nonlinear center deflections of the symmetric two layered FG laminated composite plate and the laminated composite plate ($0^\circ/90^\circ/0^\circ$) ($a/h = 100$, $a = b$) with the dimensionless intensity (Q) of uniformly distributed load and (b, c) distributions of dimensionless in-plane normal stresses ($\bar{\sigma}_x, \bar{\sigma}_y$) across the thickness of the plates.

domain using both the GHM method and the conventional complex modulus approach when the patch is passive. It should be noted here that in the finite element formulation when $[\boldsymbol{\theta}]$ is considered as a null matrix, the governing equations of motion and hence Eq. (35) become linear describing the linear behavior of the overall FG laminated composite plate. In the GHM method, the frequency response function can be computed from the following equation:

$$\{\mathbf{X}\} = ([\bar{\mathbf{K}}] - \mathrm{i}\omega[\bar{\mathbf{C}}] - \omega^2[\bar{\mathbf{M}}])^{-1}\{\bar{\mathbf{F}}\} \tag{37}$$

while, in the complex modulus approach, the same can be obtained from the following equation:

$$\{\mathbf{X}_t\} = ([\mathbf{K}(\mathrm{i}\omega) - \omega^2[\mathbf{M}]])^{-1}\{\mathbf{F}_m\} \tag{38}$$

where

$$[\mathbf{K}(\mathrm{i}\omega)] = ([\mathbf{K}_{tt}] + [\mathbf{K}^v_{tt}]G(\mathrm{i}\omega)) - ([\mathbf{K}_{tr}] + [\mathbf{K}^v_{tr}]G(\mathrm{i}\omega))([\mathbf{K}_{rr}] + [\mathbf{K}^v_{rr}]G(\mathrm{i}\omega))^{-1}([\mathbf{K}_{rt}] + [\mathbf{K}^v_{rt}]G(\mathrm{i}\omega)) \tag{39}$$

in which $G(\mathrm{i}\omega)$ is the complex shear modulus of the constrained viscoelastic layer. Considering a point transverse load ($1\,\mathrm{e}^{-\mathrm{i}\varpi t}N$) at the point ($a/4$, $b/4$, $h/2$) with ω being the driving frequency, the frequency response for the deflection at the point ($a/4$, $b/4$, $h/2$) of the overall plate computed by the two approaches are

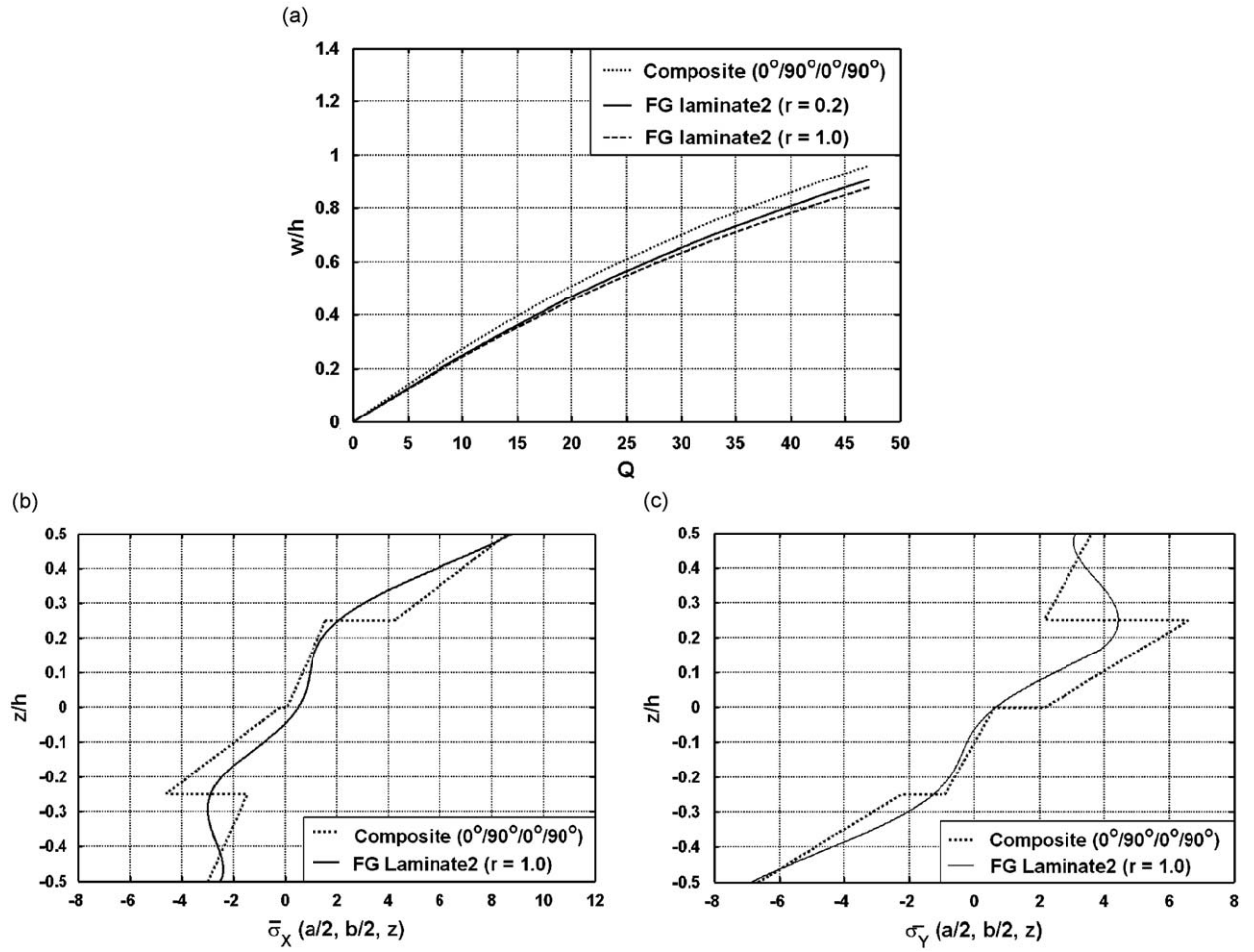

Fig. 6. (a) Variation of nonlinear center deflections of the asymmetric three layered FG laminated composite plate and the laminated composite plate $(0^\circ/90^\circ/0^\circ/90^\circ)$ $(a/h = 100,\ a = b)$ with the dimensionless intensity (Q) of uniformly distributed load and (b, c) distributions of dimensionless in-plane normal stresses $(\bar{\sigma}_x, \bar{\sigma}_y)$ across the thickness of the plates.

shown in Fig. 7(a). It may be observed that the frequency response by the GHM method with a single term GHM expression $(\alpha_1 = 2.3263 \times 10^4, \hat{\omega}_1 = 6.6169 \times 10^6, \hat{\xi}_1 = 3.0787)$ is in excellent agreement with that obtained by the complex modulus approach. Thus the present modeling of the constrained viscoelastic layer of the ACLD treatment by the GHM method accurately predicts the damping characteristics of the overall FG laminated composite plate. For further verification of the present finite element model and the numerical integration scheme implemented to compute the nonlinear transient responses, a nonlinear transient vibration analysis is carried out considering the substrate plate as an isotropic FG plate integrated with the passive $(k_d = 0)$ and negligibly thin $((h_p + h_v) \approx 0)$ ACLD patch. Using the material properties, boundary conditions and mechanical loading considered by Praveen and Reddy [13], the transient responses at the center of this FG substrate plate are computed and compared with those of an identical FG plate without integrated with the ACLD patch. This comparison is illustrated in Fig. 7(b). Excellent matching of the results can be observed from this figure verifying the present finite element model as well as the numerical integration scheme. Note that the responses presented by Praveen and Reddy [13] include the consideration of rotary inertia of the plate while the present responses do not include the effect of the rotary inertia. Thus, the comparison shown in Fig. 7 corroborates our consideration that the rotational velocities are not included in estimating the kinetic energies of the plates.

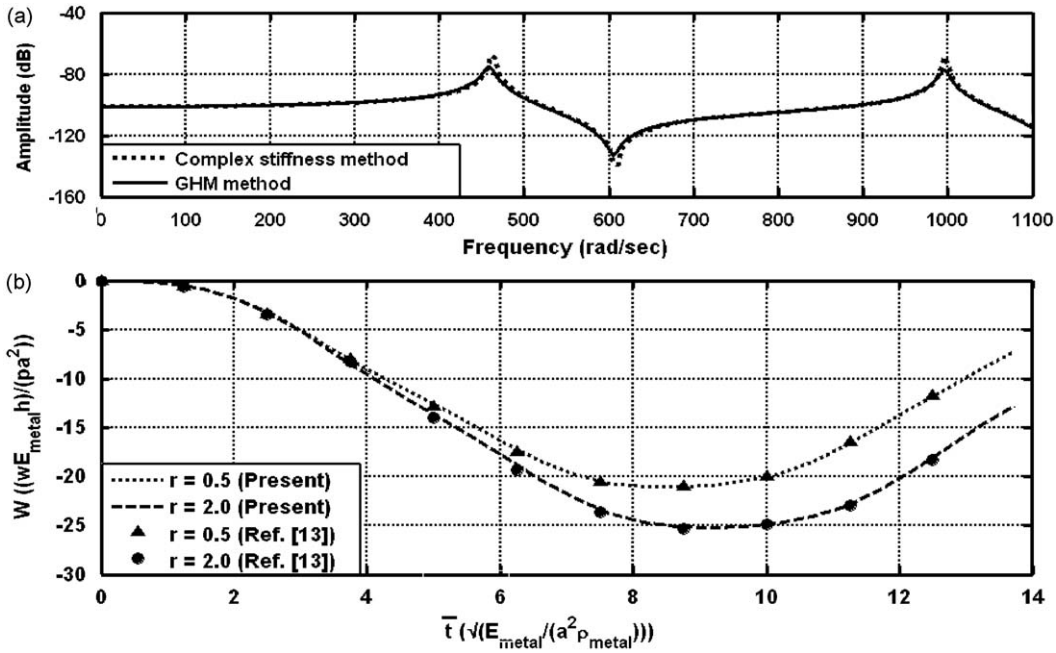

Fig. 7. Verification of the FE model: (a) the implementation of the GHM method (FG laminate 1, $a/h = 100$, $a = b$, $r = 0.5$) and (b) the numerical integration scheme [13].

In order to cause the nonlinear forced vibrations of the host FG laminated composite plates, it is required to choose the magnitude of the applied mechanical load. Such a value of the applied mechanical load can be predicted from the plots for the variation of the center deflection of the host FG laminated composite plate with the static applied mechanical load as shown in Figs. 5(a). Thus, for the computation of nonlinear transient responses of simply supported thin FG laminated composite plates, the dimensionless intensity (Q) of the uniformly distributed step load should be considered as 10 or more. To investigate the performance of the PFRC material as the active constraining layer of the ACLD treatment, the nonlinear transient responses at the mid-point of the simply supported two layered FG laminated composite plate (FG laminate 1) are computed and plotted in Fig. 8(a). As displayed in this figure, the active ($k_d \neq 0$) patch of the ACLD treatment significantly increases the damping characteristics of this overall FG laminated composite plate over the passive ($k_d = 0$) damping characteristics and this suggests the potential use of the PFRC material as the constraining layer of the ACLD treatment for controlling the nonlinear dynamics of the FG laminated composite plates. The control voltage presented in Fig. 8(b) corresponding to the gain used for the transient responses shown in Fig. 8(a), is quite low. Since the control voltage is proportional to the velocity at the center of the plate, Fig. 8(b) reveals that as the transient vibrations of the plate reduces, the velocity of the plate decays with time. The phase plot shown in Fig. 8(c) also corroborates this observation indicating the stability of the plate. Fig. 9 demonstrates that the active patch significantly annuls the geometrically nonlinear forced vibrations of the asymmetric three layered FG laminated composite plate (FG laminate 2) described in Fig. 4(a). For the constant values of the mechanical load and the velocity feed back control gain (k_d), Figs. 10 and 11 illustrate the nonlinear transient responses at the center of the FG laminates 1 and 2, respectively, for different values of power-law index r. Displayed in these figures are the corresponding responses of the conventional laminated cross-ply plates. It may be observed from these figures that for both symmetric two layered and asymmetric three layered FG laminates, the time period and amplitude of forced vibrations decrease as the power-law index r increases when compared with the conventional cross-ply plates for $\psi = 0^\circ$.

To quantify the performance of the ACLD patch for controlling the geometrically nonlinear forced vibrations of the substrate FG laminated composite plates being studied here, a performance index

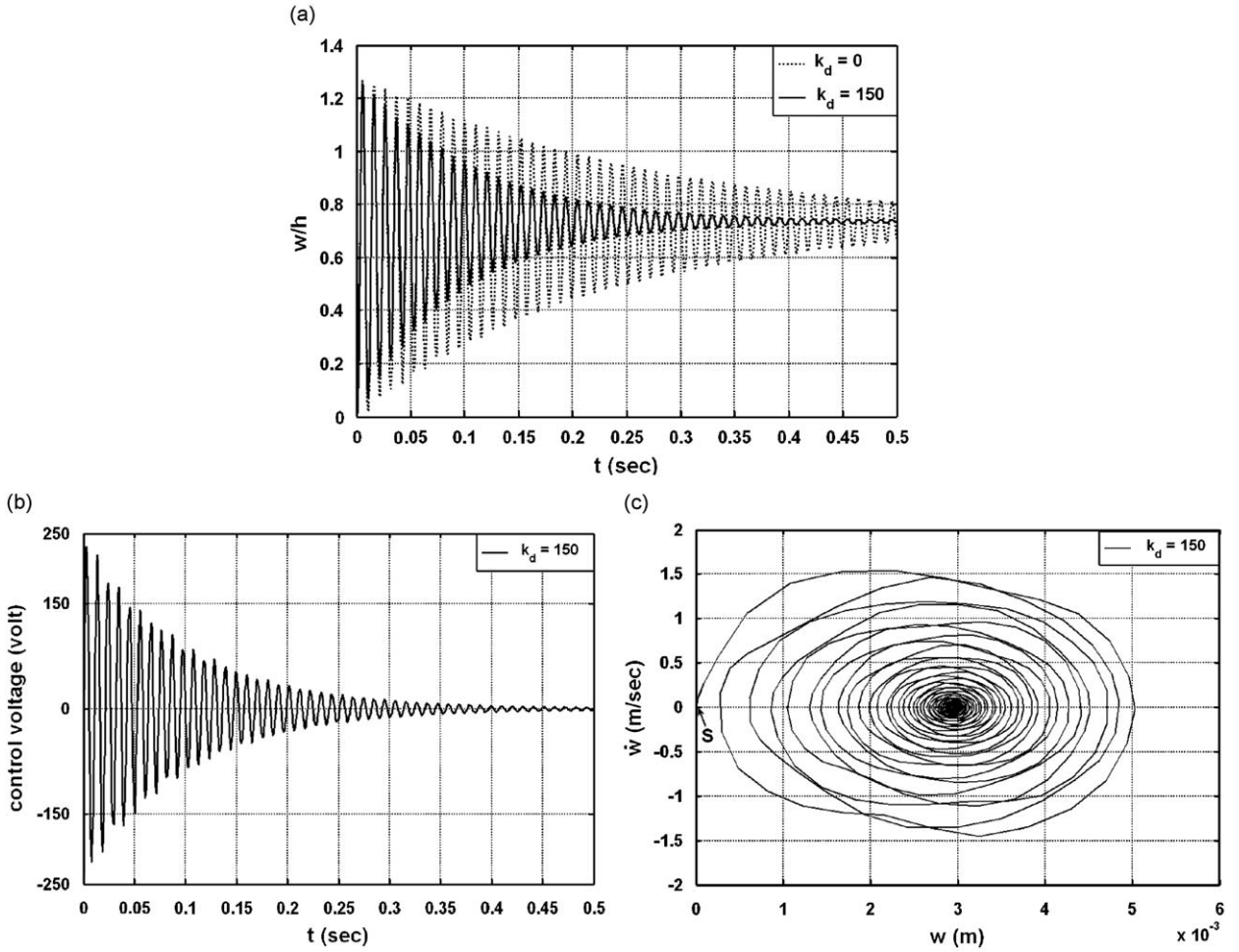

Fig. 8. Nonlinear transient responses for: (a) the center deflection of the simply supported overall symmetric FG laminated composite plate (FG laminate 1, $a/h = 100$, $a = b$, $r = 1.0$), (b) the corresponding control voltage and (c) the corresponding phase plot ("S" is the starting point of motion).

is defined as follows:

$$I_d = \frac{A_{t=0} - A_{t=0.2\,\mathrm{s}}}{A_{t=0}} \times 100 \tag{40}$$

where I_d measures the percentage diminution of amplitude of nonlinear transient vibrations of the overall plate after 0.2 s. For the constant values of mechanical load and gain, Fig. 12 illustrates the variation of this index with the piezoelectric fiber orientation angle in the constraining PFRC layer when the substrate is the FG laminate 1. Fig. 13 illustrates the same when the substrate plate is the FG laminate 2. It may be observed from these figures that in contrast to the conventional cross-ply composite plates, the performance of the ACLD patch for controlling the geometrically nonlinear forced vibrations of the overall FG laminated composite plates ($r \neq 0$) is dependent on the sign of the piezoelectric fiber orientation angle ψ in the constraining PFRC layer. The maximum values of the performance index and the corresponding value of ψ vary with the values of the power-law index (r). For $r = 0.2$, the performance of the ACLD patch becomes maximum to control both the laminates when the value of ψ is -75°. For $r = 1.0$, if the values of ψ are -30° and -60° then the performance of the patch becomes maximum to control the geometrically

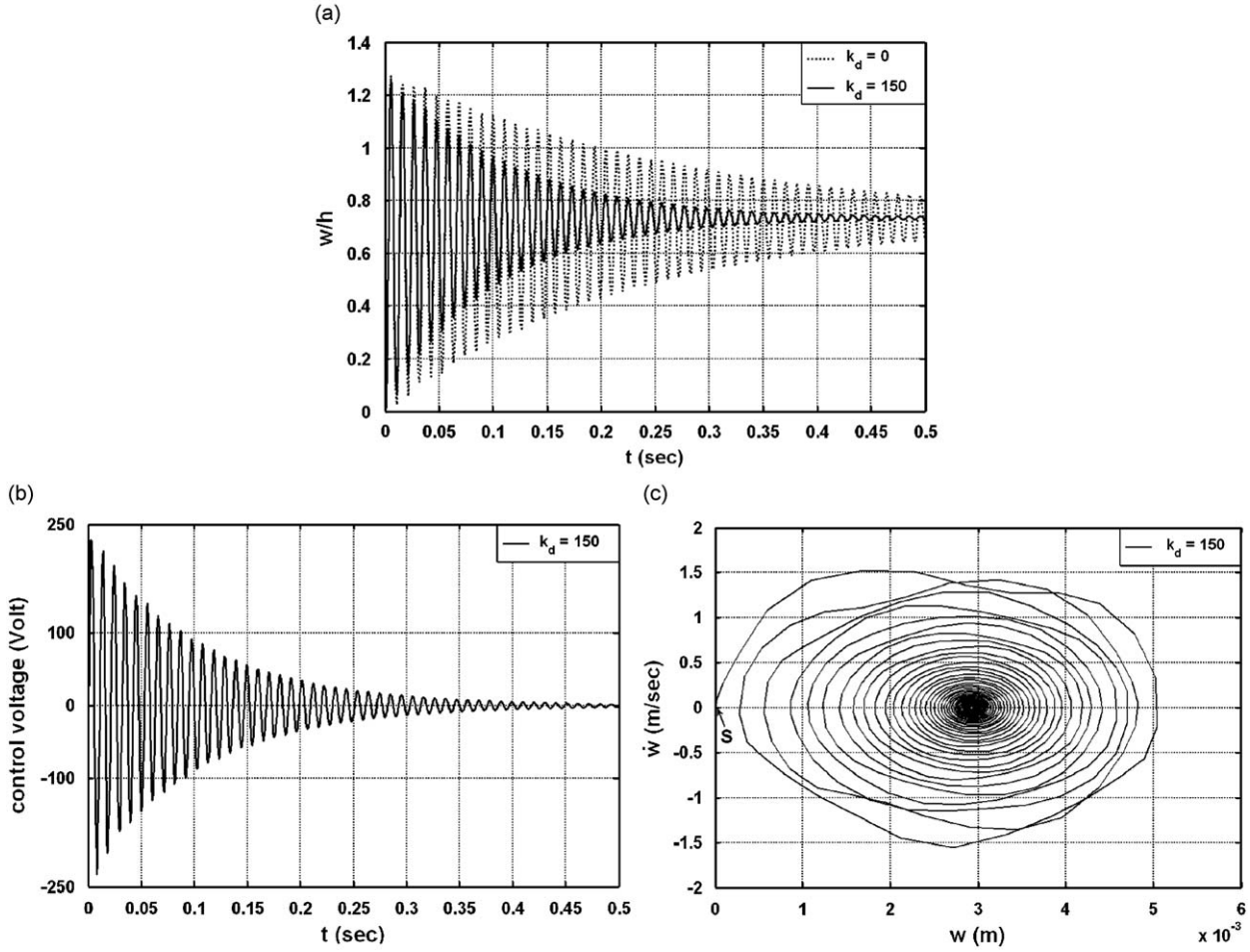

Fig. 9. Nonlinear transient responses for: (a) the center deflection of the simply supported overall asymmetric FG laminated composite plate (FG laminate 2, $a/h = 100$, $a = b$, $r = 1.0$), (b) the corresponding control voltage and (c) the corresponding phase plot ("S" is the starting point of motion).

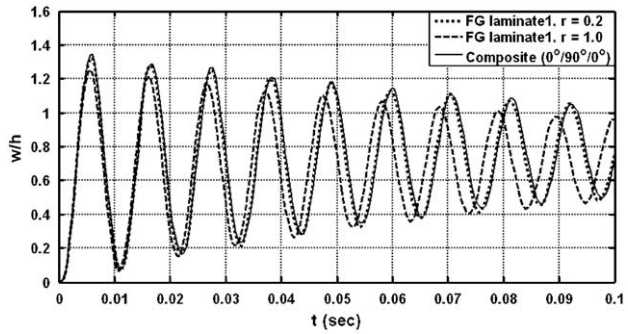

Fig. 10. Controlled transient responses at the center of the symmetric FG laminated composite plate and the laminated composite plate ($0^\circ/90^\circ/0^\circ$) ($a/h = 100$, $a = b$, $p = 4\,\mathrm{kN/m^2}$, $k_d = 150$).

nonlinear forced vibrations of FG laminates 1 and 2, respectively. Figs. 12 and 13 also reveal that the controllability of the ACLD patch can be significantly improved if the substrate FG laminated plate is optimally designed.

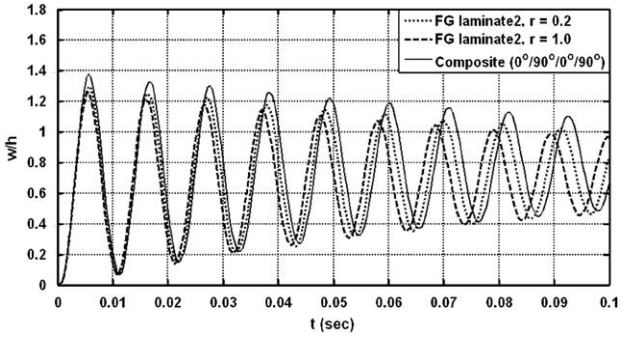

Fig. 11. Controlled transient responses at the center of the asymmetric FG laminated composite plate and the laminated composite plate $(0^\circ/90^\circ/0^\circ/90^\circ)$ ($a/h = 100$, $a = b$, $p = 4\,\mathrm{kN/m^2}$, $k_d = 150$).

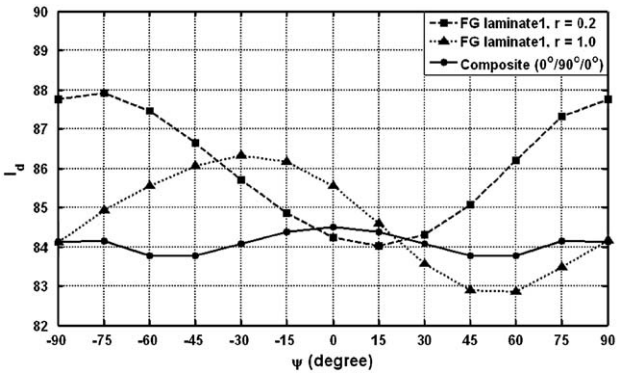

Fig. 12. Effect of piezoelectric fiber orientation angle ψ in the PFRC constraining layer of the ACLD patch on the performance of the patch for controlling geometrically nonlinear forced vibrations of the host symmetric FG laminated composite plate (FG laminate 1, $a/h = 100$, $a = b$, $p = 4\,\mathrm{kN/m^2}$, $k_d = 150$).

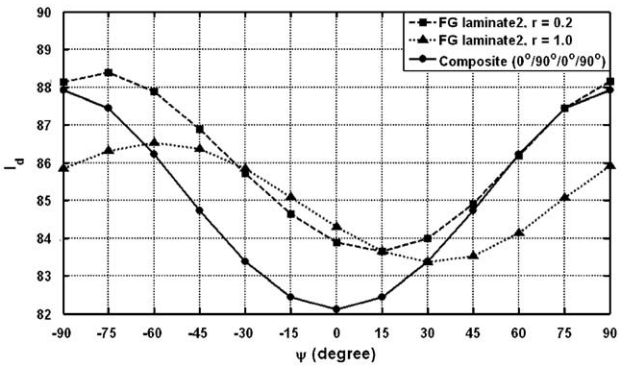

Fig. 13. Effect of piezoelectric fiber orientation angle ψ in the PFRC constraining layer of the ACLD patch on the performance of the patch for controlling geometrically nonlinear forced vibrations of the host asymmetric FG laminated plate (FG laminate 2, $a/h = 100$, $a = b$, $p = 4\,\mathrm{kN/m^2}$, $k_d = 150$).

4. Conclusion

In this paper, a finite element model has been developed to model the open-loop and closed-loop nonlinear dynamics of the FG laminated composite plates integrated with a patch of ACLD treatment. The active

constraining layer of the ACLD treatment is made of the PFRC material in order to investigate its performance as the constraining layer of the ACLD patch for controlling the nonlinear forced vibrations of the FG laminated composite plates. Each layer of the substrate FG laminated composite plate is made of generally orthotropic FG composite material in which the fibers are longitudinally aligned in the plane parallel to the top and bottom surfaces of the layer . In order to attain the graded properties along the thickness direction, the fiber orientation angle in each layer of the FG laminated plates is assumed to vary along the thickness direction according to a simple power-law. The FG layers are stacked together to form the FG laminated composite plates such that fiber orientation angles at the interface between two adjacent FG composite layers become identical and thus the continuous variation of material properties along the thickness direction is achieved. Symmetric two layered and asymmetric three layered FG laminated plates are considered for evaluating the numerical results. For the time domain analysis, the viscoelastic constrained layer of the ACLD patch is modeled by implementing the Golla–Hughes–McTavish method. The kinematics of deformations of the overall plate is based on the first-order shear deformation theory while small strains and moderate rotations are assumed for the geometric nonlinearity. The numerical results reveal that, unlike the conventional laminated composite plates, the variations of stresses across the thickness of the FG laminated composite plates are smooth and continuous. The numerical results for the dynamic analysis reveal that the patch of ACLD treatment significantly improves the damping characteristics of the FG laminated composite plates over the passive damping for controlling geometrically nonlinear forced vibrations of the plates. If the value of power-law index increases then the time period and the amplitudes of the controlled response of the FG laminated composite plates decreases for $\psi = 0^\circ$. The damping characteristics of the overall composite plate vary for different values of power-law index of the substrate FG laminated composite plate. More importantly, unlike the conventional laminated cross-ply composite plates, the performance of the ACLD patch for controlling the nonlinear forced vibrations of the FG laminated composite plates is sensitive to the variation of sign of the piezoelectric fiber orientation angle in the active PFRC constraining layer. The present investigations reveal that the optimization of the fiber orientation angle in the FG orthotropic layers should be accomplished to design FG laminated composite plates such that the controllability of the ACLD patch to control such FG laminated composite plates becomes significantly larger than that to control the conventional cross-ply composite plates of identical geometry and material.

References

[1] M. Koizumi, Concept of FGM, *Ceramic Transaction* 34 (1993) 3–10.
[2] E. Feldman, J. Aboudi, Buckling analysis of functionally graded plates subjected to uniaxial loading, *Composite Structures* 38 (1997) 29–36.
[3] A.M. Mian, A.J.M. Spencer, Exact solutions for functionally graded and laminated elastic materials, *Journal of the Mechanics and Physics of Solids* 46 (1998) 2283–2295.
[4] B.V. Sankar, An elasticity solution for functionally graded beams, *Composite Science and Technology* 61 (2001) 689–696.
[5] R.C. Batra, S.S. Vel, Exact solution for thermoelastic deformations of functionally graded thick rectangular plates, *AIAA Journal* 40 (2001) 1421–1433.
[6] Z. Zhong, E.T. Shang, Three dimensional exact analysis of a simply supported functionally gradient plate, *International Journal of Solids and Structures* 40 (2003) 5335–5352.
[7] C.T. Loy, K.Y. Lam, J.N. Reddy, Vibration of functionally graded cylindrical shells, *International Journal of Mechanical Sciences* 41 (1999) 309–324.
[8] Y.Y. Yang, Time-dependent stress analysis in functionally graded materials, *International Journal of Solids and Structures* 37 (2000) 7593–7608.
[9] J. Yang, H.S. Shen, Dynamic response of initially stressed functionally graded rectangular thin plates, *Composite Structures* 54 (2001) 497–508.
[10] S.S. Vel, R.C. Batra, Three-dimensional analysis of transient thermal stresses in functionally graded plates, *International Journal of Solids and Structures* 40 (2003) 7181–7196.
[11] A. Chakraborty, S. Gopalakrishnan, J.N. Reddy, A new beam finite element for the analysis of functionally graded materials, *International Journal of Mechanical Sciences* 45 (2003) 519–539.
[12] B. Chen, L. Tong, Y. Gu, H. Zhang, O. Ochoa, Transient heat transfer analysis of functionally graded materials using adaptive precise time integration and graded finite elements, *Numerical Heat Transfer—Part B: Fundamentals* 45 (2004) 181–200.
[13] G.N. Praveen, J.N. Reddy, Nonlinear transient thermoelastic analysis of functionally graded ceramic metal plates, *International Journal of Solids and Structures* 35 (1998) 4457–4476.

[14] J. Woo, S.A. Meguid, Nonlinear analysis of functionally graded plates and shallow shells, *International Journal of Solids and Structures* 38 (2001) 7409–7421.
[15] H.S. Shen, Nonlinear bending response of functionally graded plates subjected to transverse loads and in thermal environments, *International Journal of Mechanical Sciences* 44 (2002) 561–584.
[16] T. Bailey, J.E. Hubbard, Distributed piezoelectric polymer active vibration control of a cantilever beam, *Journal of Guidance, Control and Dynamics* 8 (1985) 605–611.
[17] S.E. Miller, J.E. Hubbard, Observability of a Bernoulli–Euler beam using PVF_2 as a distributed sensor, MIT Draper Laboratory Report, July 1, 1987.
[18] K.M. Liew, X.Q. He, T.Y. Ng, S. Kitipornchai, Finite element piezo-thermo-elasticity analysis and active control of FGM plates with integrated piezoelectric sensors and actuators, *Computational Mechanics* 31 (2003) 350–358.
[19] J. Yang, S. Kitipornchai, K.M. Liew, Non-linear analysis of thermo-electro-mechanical behavior of shear deformable FGM plates with piezoelectric actuators, *International Journal for Numerical Methods in Engineering* 59 (2004) 1605–1632.
[20] X.-L. Huang, H.-S. Shen, Vibration and dynamic response of functionally graded plates with piezoelectric actuators in thermal environments, *Journal of Sound and Vibration* 289 (2006) 25–53.
[21] A. Baz, J. Ro, Optimum design and control of active constrained layer damping, *ASME Journal of Vibrations and Acoustics* 117B (1995) 135–144.
[22] A. Baz, J. Ro, Vibration control of plates with active constrained layer damping, *Smart Materials and Structures* 5 (1995) 272–280.
[23] M.C. Ray, A. Baz, Optimization of energy dissipation of active constrained layer damping treatment of plates, *Journal of Sound and Vibration* 208 (1997) 391–406.
[24] M.J. Lam, D.J. Inman, W.R. Saunders, Hybrid damping models using the Golla–Hughes–McTavish method with internally balanced model reduction and output feedback, *Smart Materials and Structures* 9 (2000) 362–371.
[25] M.C. Ray, J. Oh, A. Baz, Active constrained layer damping of thin cylindrical panels, *Journal of Sound and Vibration* 240 (2001) 921–935.
[26] Y.-H. Lim, V.V. Varadan, V.K. Varadan, Closed-loop finite element modeling of active constrained layer damping in the time domain analysis, *Smart Materials and Structures* 11 (2002) 89–97.
[27] Y. Shi, H. Hua, H. Sol, The finite element analysis and experimental study of beams with active constrained layer damping treatments, *Journal of Sound and Vibration* 278 (2004) 343–363.
[28] M.C. Ray, Micromechanical analysis of piezoelectric fiber reinforced composites with improved effective piezoelectric constant, *International Journal of Mechanics and Materials in Design* 3 (2007) 361–371.
[29] N. Mallik, M.C. Ray, Effective coefficients of piezoelectric fiber reinforced composites, *AIAA Journal* 41 (2003) 704–710.
[30] M.C. Ray, H.M. Sachade, Exact solutions for the functionally graded plates integrated with a layer of piezoelectric fiber-reinforced composite, *ASME Journal of Applied Mechanics* 73 (2006) 622–632.
[31] S. Panda, M.C. Ray, Nonlinear analysis of smart functionally graded plates integrated with a layer of piezoelectric fiber reinforced composite, *Smart Materials and Structures* 15 (2006) 1595–1604.
[32] M.C. Ray, Hybrid damping of smart functionally graded plates using piezoelectric fiber reinforced composites, *IEEE Transactions on Ultrasonics, Ferroelectrics, and Frequency Control* 53 (2006) 2152–2165.
[33] S. Panda, M.C. Ray, Active constrained layer damping of geometrically nonlinear transient vibrations of smart functionally graded plates using piezoelectric fiber reinforced composite, *Smart Materials and Structures* 17 (2008) Art no. 025012.
[34] D.F. Golla, P.C. Hughes, Dynamics of viscoelastic structures: a time-domain, finite element formulation, *ASME Journal of Applied Mechanics* 52 (1985) 897–906.
[35] D.J. McTavish, P.C. Hughes, Modeling of linear viscoelastic space structures, *ASME Journal of Vibration and Acoustics* 115 (1993) 103–133.
[36] J.N. Reddy, *An Introduction to Nonlinear Finite Element Analysis*, Oxford University Press Inc., New York, 2004.
[37] R.M. Christensen, *Theory of Viscoelasticity: An Introduction*, second ed., Academic Press, New York, 1982.
[38] H.F. Tiersten, *Linear Piezoelectric Plate Vibrations*, Plenum Press, New York, 1969.
[39] T.-W. Kim, J.-H. Kim, Nonlinear vibration of viscoelastic laminated composite plates, *International Journal of Solids and Structures* 39 (2002) 2857–2870.
[40] S. Benmedakhene, M. Kenane, M.L. Benzeggagh, Initiation and growth of delamination in glass/epoxy composites subjected to static and dynamic loading by acoustic emission monitoring, *Composites Science and Technology* 59 (1999) 201–208.